Equilibrium and dynamics of uniform density ellipsoidal non-neutral plasmas

D. H. E. Dubin
Department of Physics, University of California at San Diego, La Jolla, California 92093-0319

(Received 29 June 1992; accepted 15 October 1992)

When a single-species plasma is confined in a harmonic Penning trap at cryogenic temperature, the thermal equilibrium is approximately a uniform density spheroid (ellipsoid of revolution). Normal modes corresponding to quadrupole excitations of this plasma have recently been measured. In this paper, nonlinear equations of motion are derived for these quadrupole oscillations. For large amplitudes, the oscillations deform a spheroidal plasma into a triaxial ellipsoid with time-dependent shape and orientation. The integrals of the motion are found and the cylindrically symmetric finite-amplitude oscillations of a spheroid are studied. An analysis of all possible ellipsoidal equilibria is also carried out. New equilibria are discovered which correspond to finite-amplitude versions of the noncylindrically symmetric linear quadrupole oscillations. The equilibria are shown to fall into two classes in which the ellipsoids are either tilted or aligned with respect to the magnetic field. Some of these equilibria have densities well above the Brillouin limit.

I. INTRODUCTION

In recent experiments[1] at the National Institute of Standards and Technology (NIST), a pure ion plasma consisting of $N \simeq 10^2$–10^4 singly ionized beryllium ions is confined in a Penning trap and laser cooled to temperatures in the milliKelvin range. The ions can be trapped for long periods of time, approaching a confined thermal equilibrium state.[2] The temperature T of this thermal equilibrium is sufficiently small and both the particle number N and the density n are sufficiently large so that both the Debye length $\lambda_D = (kT/4\pi q^2 n)^{1/2}$ and the average interparticle spacing $n^{-1/3}$ are much smaller than the size of the plasma (here q is the ion charge). However, the plasma itself is much smaller than the distance to the trap electrodes (see Fig. 1), so that induced image charges in the electrodes have a negligible effect on the plasma dynamics, and the electrostatic confinement potential is harmonic. Under these conditions the thermal equilibrium state can be described by a cold-fluid theory[3,4] in which the plasma is a uniform density spheroidally shaped cloud of charge, rotating rigidly about the axis of symmetry of the trap. This cold-fluid model of the thermal equilibrium state has been verified experimentally.[1]

Normal modes of oscillation have recently been excited in such a small cold spheroidal plasma,[5] and detected using a laser fluorescence diagnostic technique. The particular modes that were excited in the experiments were quadrupole oscillations of the plasma, in which the perturbed oscillating potential has a quadratic dependence on position within the cloud, and the density within the plasma remains uniform in space (but may oscillate in time). A simple analytic theory of the linear electrostatic cold-fluid modes of the plasma has been developed[6] which matches the experimental results well. The detection of normal modes has been proposed[5–7] as a probe of plasma properties such as density and temperature. This technique may be particularly useful as a nondestructive diagnostic for plasmas such as electron, positron,[8] or antiproton[9] plasmas, which cannot be observed using laser fluorescence techniques. However, if the modes are detected through the image charges they create in the trap electrodes, and if the plasma is small compared to the diameter of the electrodes, it may be difficult to observe the modes unless they are excited to large amplitude where nonlinear effects are important.

In this paper, we consider the nonlinear behavior of the quadrupole oscillations of a cold spheroidal non-neutral plasma. We find that, for these quadrupole oscillations, the nonlinear ideal cold-fluid equations can be reduced to a simple Hamiltonian system of coupled ordinary differential equations. Our results predict nonlinear frequency shifts and stochastic behavior of the oscillations. Furthermore, we find that solutions exist for which the plasma shape is stationary in some rotating frame. For some of these rotating equilibria, the plasma density is considerably larger than the Brillouin limit condition[10] given by $\omega_p^2 \leqslant \Omega_c^2/2$, where $\omega_p = (4\pi q^2 n/m)^{1/2}$ is the plasma frequency, $\Omega_c = qB/mc$ is the cyclotron frequency, B is the magnitude of the applied magnetic field, and m is the mass of an ion. These high density states can occur because the plasma is not cylindrically symmetric, and it does not rotate rigidly. Rather, sheared fluid flow within the ellipsoid can provide an extra confining Lorentz force not present in rigidly rotating systems.

Before we proceed with a description of the nonlinear quadrupole motions, we briefly review the confinement characteristics of Penning traps. Penning traps are employed in a number of disciplines, ranging from atomic physics to ion chemistry, and the confinement properties of non-neutral plasmas in such traps have been studied extensively. One simple version of a Penning trap consists of three cylindrically symmetric electrodes immersed in an applied uniform magnetic field oriented along the axis of symmetry (see Fig. 1). In fact, cylindrically symmetric electrodes are not always employed, and are not a neces-

 0899-8221/93/020295-30$06.00

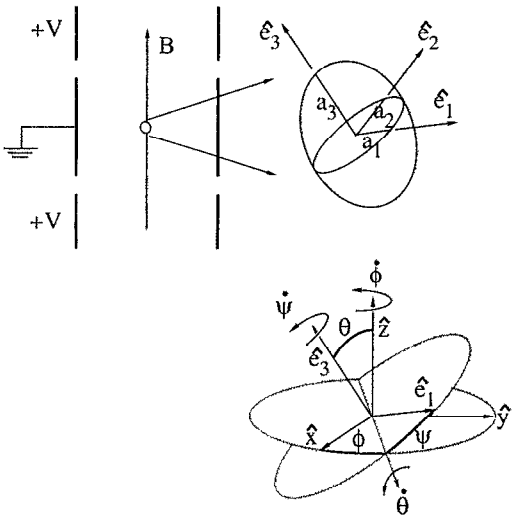

FIG. 1. Schematic of the confinement geometry. The plasma is confined by the potentials applied to three cylindrical electrodes, and a uniform magnetic field. To the right of the schematic, a blowup of the plasma shows the three unit vectors $\hat{\mathbf{e}}_1$, $\hat{\mathbf{e}}_2$, and $\hat{\mathbf{e}}_3$, which are oriented along the body axes, and below this blowup is displayed the relation between $(\hat{\mathbf{e}}_1,\hat{\mathbf{e}}_2,\hat{\mathbf{e}}_3)$ and the laboratory axes $(\hat{\mathbf{x}},\hat{\mathbf{y}},\hat{\mathbf{z}})$ in terms of three successive rotations by Euler angles ϕ, θ, and ψ, respectively.

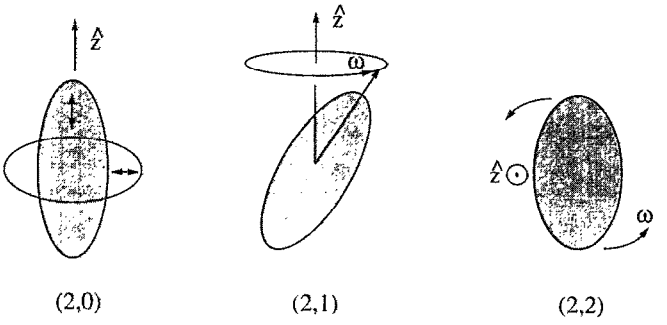

FIG. 2. Schematic of the three normal modes of oscillation. The (2,0) mode is an oscillation in the length and radius of a spheroid whose axis of symmetry is oriented along the z direction. The (2,1) mode is a slight tilt of the plasma with respect to z; the tilted plasma then precesses around the z axis with angular phase velocity ω. In the (2,2) mode, the plasma is slightly distorted into a triaxial ellipsoid with a principal axis along the z direction. The ellipsoid then rotates around the z-axis with phase velocity ω. The motions considered in this paper are finite-amplitude extensions of these modes.

sary assumption in our analysis. However, we consider only this case in this paper in order to simplify the results.

Confinement of the plasma in the direction parallel to the magnetic field (referred to throughout the paper as the laboratory z direction) is provided by dc voltages applied to the two end electrodes with respect to the central electrode. This creates a potential well in the z direction, which for a small plasma can be approximated over the volume of the plasma by the first nonzero terms in the Taylor expansion around the saddle point of the potential:

$$\phi_e=\frac{1}{2}\frac{m}{q}\omega_z^2\left(z^2-\frac{1}{2}(x^2+y^2)\right), \tag{1}$$

where ω_z is the frequency of oscillation of a single particle in the z direction, and (x,y,z) are Cartesian coordinates taken with respect to fixed laboratory axes, and measured from the center of the trap. This potential is an excellent approximation for the NIST experiments, where the diameter of the trap electrodes is about 25 mm, but the plasma size is less than about 1 mm, and the electrodes have been designed to minimize anharmonic corrections to the potential.

The trap potential ϕ_e provides confinement only in the z direction. Confinement of the plasma in the radial direction is furnished by the uniform applied magnetic field, $\mathbf{B}=B\hat{\mathbf{z}}$. The plasma rotates through this magnetic field, inducing a confining $\mathbf{v}\times\mathbf{B}$ force that balances the centrifugal force due to rotation as well as the repulsive radial electric force of the external trap field and the plasma space charge.

The plasma can be confined for very long periods of time in such a trap, and so interparticle interactions cause the plasma to relax toward a confined thermal equilibrium state. The thermal equilibrium state is characterized by a uniform temperature T as well as a uniform rotation frequency ω. If both λ_D and $n^{-1/3}$ are small compared to the size of the plasma, one may neglect the effects of finite temperature and correlations on the thermal equilibrium state and, to lowest order in these small quantities, the resulting cold-fluid equilibrium can be shown to be a uniform density spheroid.[3,4] We will discuss the properties of this rigidly rotating spheroid in the next section as well as in Sec. III, where it appears as a special case of more general ellipsoidal fluid equilibria.

When ϕ_e is perturbed slightly (for example, through a small time-dependent variation of the electrode voltages), small-amplitude oscillations of the plasma spheroid are set up, which can be treated using linear fluid theory. In this paper, we focus on the quadrupole oscillations, since they have been observed experimentally[5] and, as we will see, they have a particularly simple theoretical description. There are three types of quadrupole oscillations, shown in Fig. 2, and designated (2,0), (2,1), and (2,2) modes. The second index refers to the number of zeros in the mode potential as a function of azimuthal angle ϕ, whereas the difference between the first and second indices refers to the number of zeros in the potential as one proceeds from pole to pole along the spheroid surface.[6]

The (2,0) oscillations are cylindrically symmetric oscillations in the length and radius of the spheroid. When $\Omega_c \gg \omega_p$, the radial oscillation is nearly at Ω_c and is referred to as an upper-hybrid mode. The axial oscillation is at a frequency on the order of ω_p, and is a magnetized plasma mode. The (2,1) mode sets up a perturbed potential within the plasma with spatial variation $z(x+iy)$; that is, the x and y motions are $\pi/2$ out of phase. This potential corresponds to a spheroid that is slightly tilted with respect to the z axis, and which then precesses around the z axis, as shown in Fig. 2(b). There are three possible precession rates; when $\Omega_c \gg \omega_p$, two are of order ω_p and one is near Ω_c. The (2,2) perturbed mode potential within the plasma var-

ies as $(x+iy)^2$. This potential corresponds to a plasma that has been flattened slightly into a triaxial ellipsoid with a principal axis oriented along z. This ellipsoid then rotates around the z axis, as shown in Fig. 2(c), at one of two possible frequencies; when $\Omega_c \gg \omega_p$ one is of order ω_p^2/Ω_c and one is near Ω_c.

When these normal modes are excited to finite amplitude, we find that they can be described by a Hamiltonian system of equations with nine degrees of freedom. These nine degrees of freedom have the following simple interpretations. During the quadrupole motions the plasma can distort into a triaxial ellipsoid, described by the equation

$$\frac{x_1^2}{a_1^2}+\frac{x_2^2}{a_2^2}+\frac{x_3^2}{a_3^2}=1, \tag{2}$$

where the x_i's are Cartesian coordinates measured from the center of the cloud with respect to the ellipsoid's principal axes, which are oriented in directions defined by the orthogonal unit vectors $\hat{\mathbf{e}}_i$ (see Fig. 1). Throughout the paper, the subscript i, $i=1$–3, denotes components taken with respect to principal axes. The lengths of these axes, a_1, a_2, and a_3, are not necessarily equal and may be functions of time; (a_1,a_2,a_3) are the first three degrees of freedom. Furthermore, we will see that the ellipsoid can rotate with rotation frequency $\boldsymbol{\omega}$, which introduces another three degrees of freedom; that is, the three Euler angles (θ,ϕ,ψ) required to determine the orientation of the principal axes with respect to a fixed laboratory frame (see Fig. 1). Finally, the plasma within this triaxial ellipsoid need not rotate rigidly, and, in fact, can circulate in a manner described by the vorticity vector $\boldsymbol{\zeta}=\nabla\times\mathbf{v}_r$, where $\mathbf{v}_r$ is the fluid velocity as seen in the frame rotating with the body axes. The vorticity turns out to be spatially uniform within the plasma but can have any direction and magnitude. This introduces three more degrees of freedom. We will see that these degrees of freedom can be represented by three fluid Euler angles (ϕ_f,θ_f,ψ_f) describing the rotation of a fluid element with respect to the body axes.

After we determine the equations of motion for these nine degrees of freedom, we consider the integrals of the motion. We find that the only invariants are the total energy, the component of canonical angular momentum along the magnetic field, and three other constants related to the invariance of the canonical circulation in an ideal fluid.[11] These five invariants are not sufficient to reduce the system to quadratures, and, in general, the behavior is stochastic.

However, for certain special initial conditions, the dimensionality of the system can be further reduced. In particular, if initial conditions are chosen such that the ellipsoid is oriented with a principal axis along the magnetic field, and if both $\boldsymbol{\zeta}$ and $\boldsymbol{\omega}$ are also initially oriented along the magnetic field, we show that these orientations are invariant under the subsequent dynamics. By substituting the integral invariants into the equations of motion, the system can then be reduced to one with only three degrees of freedom—the lengths of the principal axes (a_1,a_2,a_3), which satisfy coupled nonlinear oscillator equations. Finally, if we assume that $a_1=a_2$, the system reduces to two coupled oscillator equations for a_1 and a_3, which describe oscillations of the radius and length of a spheroidal plasma that is oriented with the axis of symmetry along the magnetic field. When these oscillations have small amplitude, they correspond to the linear cylindrically symmetric (2,0) normal modes of the plasma spheroid [Fig. 2(a)]. This system has only one remaining invariant—the energy—and so is still not integrable. However, if the cyclotron frequency is large, the frequency of the oscillations in the radius of the spheroid is much higher than that in the length, and so an adiabatic invariant exists—the radius of the spheroid is approximately constant. This is just the $\mathbf{E}\times\mathbf{B}$ drift limit of the dynamics, in which the mean-square radius of the system is constant. This approximation allows us to reduce the system to quadratures, and so we obtain simple equations for the nonlinear frequency shift of the axial (2,0) plasma oscillation.

The (2,1) and (2,2) normal modes have equally simple finite-amplitude forms. Both the (2,1) and (2,2) linear modes appear to be stationary distortions of the plasma shape in a frame rotating with the mode angular phase velocity. The large-amplitude versions of these modes can therefore be analyzed as equilibria of our Hamiltonian system as seen in a rotating frame in which the principal axes are fixed (sometimes referred to as the body frame). Our analysis of these "fixed points" reveals a range of nonlinear equilibrium states that connect smoothly onto the linear (2,1) and (2,2) modes as the distortion of the plasma shape away from a rigid-rotor spheroid is reduced. We find that these equilibria break into two classes. In the first class, the plasma has a principal axis oriented along $\hat{\mathbf{z}}$ and both $\boldsymbol{\zeta}$ and $\boldsymbol{\omega}$ are also aligned with $\hat{\mathbf{z}}$. We refer to this class of solutions as aligned ellipsoids. These are finite-amplitude versions of (2,2) normal modes. In the second class, the ellipsoids principal axes may be tilted with respect to the magnetic field by some finite angle, and $\boldsymbol{\zeta}$ need not point in the z direction. We refer to this class of solutions as tilted ellipsoids. These solutions are finite-amplitude versions of the (2,1) normal modes.

One important set of equilibria falling in the class of tilted ellipsoid solutions consist of triaxial ellipsoids whose body axes are stationary in the laboratory frame, but in which the plasma continues to circulate with respect to the stationary axes. These stationary figures, which we refer to as Dedekind ellipsoids for reasons that will become apparent presently, may play an important role in transport processes caused by external nonaxisymmetric fields, since these time-independent states can be driven resonantly by a static external field error.[5–7]

The theory of the equilibrium and dynamics of a non-neutral plasma is similar in some important respects to the theory of what might at first seem to be a quite different system—rotating self-gravitating masses, such as stars, gas clouds, or galaxies. This analogy is well known but has not been fully exploited previously. In both the non-neutral and self-gravitating systems the interparticle force is an inverse square law, albeit with opposite signs in the two cases (which changes many of the results). Furthermore, the Coriolis force that appears in the body frame of a ro-

tating self-gravitating mass acts like the applied magnetic field in a non-neutral plasma. The equations that govern the motion of a constant density ellipsoidal plasma are therefore similar to those governing the motion of a constant density ellipsoidal self-gravitating mass (although our equations have extra terms due to the external confining trap fields). The theory of such motions extends back several hundred years to Newton's inquiries into the shape of a rotating planetary body. It was Dirichlet who first posed the question that comes closest to the subject of our paper. He inquired as to how a constant density self-gravitating fluid mass can maintain an ellipsoidal shape with internal motions that are linear functions of position. The most comprehensive review of this subject is contained in Chandrasekhar's well-known treatise entitled "Ellipsoidal Figures of Equilibrium."[12] We exploit some of the mathematical techniques reviewed in this text, and which were developed by Riemann, among others, to solve Dirichlet's problem. Some of our results are quite similar; for example, the Dedekind ellipsoids—stationary figures that incorporate internal fluid motions—exist in both problems. Our proof of the non-neutral plasma version of Riemann's theorem is similar to the proof found in Chandrasekhar, and our formulation of the equations of motion is also somewhat similar to that found in this useful text. On the other hand, our determination of the integral invariants of the motion follows a more deductive approach that exploits the underlying Hamiltonian structure of the equations, and the greater complexity of our results for the regimes of existence of equilibrium solutions requires a different mathematical attack based on a combination of numerical and analytic techniques. Also, we find that Dedekind's theorem does not apply to the non-neutral system, and none of the Jacobi ellipsoids exist except for the trivial case of the rigid-rotor thermal equilibrium spheroid. (The Jacobi ellipsoids have rotating boundaries with respect to which the fluid is stationary—that is, they are rigidly rotating triaxial ellipsoids. Such states would be nonaxisymmetric zero temperature fluid thermal equilibria, which are impossible for a non-neutral plasma confined in a cylindrical Penning trap.[13])

In Sec. II, we consider the motion of a uniform density ellipsoidal non-neutral plasma. In Sec. II A, we obtain the equations of motion, and in Sec. II B we derive the integrals of the motion. In Sec. II C, we consider two simplified equations of motion that may be obtained from the general equations for special initial conditions. The simplest of these two reduced systems describes radial and axial oscillations of a spheroidal plasma, which reduce to the (2,0) normal modes in the limit of small-oscillation amplitude. In Sec. II D we outline a simple model for the effect of finite temperature on the oscillations.

Section III deals with the equilibrium solutions of the equations of motion. In Sec. III A, we derive the conditions for ellipsoidal fluid equilibrium, including a general relation between the plasma frequency and the fluid velocity, and we prove the non-neutral plasma version of Riemann's theorem, which allows us to classify equilibria as either aligned or tilted ellipsoids. In Sec. III B, we consider the aligned ellipsoids for which $\boldsymbol{\omega}$ is parallel to $\hat{\mathbf{z}}$, $\boldsymbol{\zeta}$ is parallel to $\hat{\mathbf{z}}$, and a principal axis is along $\hat{\mathbf{z}}$. (In the astrophysics literature, these are referred to as S-type ellipsoids.) In Sec. III C, we consider the tilted ellipsoids for which $\boldsymbol{\omega}$ is again parallel to $\hat{\mathbf{z}}$, but $\boldsymbol{\zeta}$ and $\boldsymbol{\omega}$ are not parallel, falling instead in a principal plane of the ellipsoid. (In the gravitational problem, the results are quite different and the ellipsoids are classed into three types that have no analogy here.) We classify the regimes of existence of solutions for the tilted ellipsoids, finding that solutions exist only over certain ranges of a_2/a_1 and a_3/a_1, which depend on the relative magnitude of the external magnetic field and the external electrostatic trap field. We also consider the special case of the Dedekind ellipsoids that are stationary in the laboratory frame.

In Sec. IV, we review our results and examine several critical questions that will be considered in following papers. In Appendix A, we list some of the known relations for the interior electrostatic potential in a homogeneous ellipsoid. In Appendix B, we provide a list of the variables that we have employed, and the notation we have adopted.

II. DYNAMICS OF A UNIFORM DENSITY ELLIPSOIDAL NON-NEUTRAL PLASMA

A. Equations of motion

In this subsection, we derive self-consistent nonlinear equations of motion for a uniform density ellipsoidal non-neutral plasma. We describe this motion in the ideal cold-fluid approximation encompassed by the pressureless Euler equation

$$\frac{\partial \mathbf{v}}{\partial t}+\mathbf{v}\cdot\nabla\mathbf{v}=\frac{q}{m}\mathbf{E}-\Omega_c\hat{\mathbf{z}}\times\mathbf{v}, \tag{3a}$$

and the continuity equation

$$\frac{\partial n}{\partial t}+\nabla\cdot(n\mathbf{v})=0, \tag{3b}$$

where $\mathbf{v}(\mathbf{x},t)$ is the fluid velocity and $n(\mathbf{x},t)$ is the plasma density. The cyclotron frequency Ω_c is assumed to be constant, and the electric field $\mathbf{E}$ consists of the sum of the external trap field $-\nabla\phi_e$ and the field due to space charge, which we write as $-\nabla\phi_p$, where ϕ_p is the space-charge potential. A critical observation, upon which all of our results hinge, is that, in a homogeneous ellipsoidal plasma confined in the external potential ϕ_e given by Eq. (1), the electric field within the plasma is a linear function of position. We will find it useful to write the external trap field in terms of a matrix equation:

$$-\nabla\phi_e=(m/q)\omega_z^2\boldsymbol{\epsilon}_e\cdot\mathbf{x}, \tag{4a}$$

where $\boldsymbol{\epsilon}_e$ is a dimensionless tensor with a diagonal form in the laboratory frame of reference:

$$\boldsymbol{\epsilon}_e=\begin{pmatrix}\frac{1}{2} & 0 & \\ & \frac{1}{2} & \\ 0 & & -1\end{pmatrix}. \tag{4b}$$

The space-charge field also takes on a well-known form inside a homogeneous ellipsoid:[12,14]

$$-\nabla\phi_p=(m/q)\omega_p^2\epsilon_p\cdot\mathbf{x}, \tag{5a}$$

where ϵ_p is also a dimensionless symmetric tensor that has a diagonal form in coordinates aligned with the principal axes of the ellipsoid (i.e., body axes):

$$\epsilon_p'=\tfrac{1}{2}\begin{pmatrix} A_1 & & 0 \\ & A_2 & \\ 0 & & A_3 \end{pmatrix}, \tag{5b}$$

and where the prime denotes the particular representation in terms of body axes coordinates. [Throughout the paper, a prime on a vector or tensor implies that components are taken with respect to the body axes unit vectors $(\hat{\mathbf{e}}_1,\hat{\mathbf{e}}_2,\hat{\mathbf{e}}_3)$.] The functions $A_i(a_2/a_1,a_3/a_1)$ are the normalized components of the space-charge electric field taken along the body axes, and can be written in terms of special functions as listed in Appendix A. In Appendix A, we also review several useful relations between the A_i's. For future reference, we sometimes write A_i as a function of a single variable a_3/a_1, by which we mean the spheroidal form should be used with $a_2=a_1$.

Since the electric field is a linear function of position within the ellipsoid, the form of Eq. (3) suggests that, in order to obtain simple closed equations for the fluid velocity, we assume that the velocity is also linear in the coordinates,

$$\mathbf{v}(\mathbf{x},t)=\mathbf{W}(t)\cdot\mathbf{x}, \tag{6}$$

where $\mathbf{W}$ is a 3×3 matrix which we refer to as the velocity tensor. This is the form of the fluid velocity in a linear quadrupole mode,[5-7] but we will keep the nonlinear terms in the equations of motion as well. Substituting Eq. (6) into Eq. (3a), and stripping away the linear $\mathbf{x}$ dependence of the resulting equation then yields a nonlinear matrix equation for the components of $\mathbf{W}$:

$$\dot{\mathbf{W}}+\mathbf{W}\cdot\mathbf{W}=\omega_z^2\epsilon_e+\omega_p^2\epsilon_p-\Omega_c\hat{\mathbf{z}}\times\mathbf{W}. \tag{7}$$

By removing the variable $\mathbf{x}$ has been removed from the fluid equations and we have reduced Eq. (3a) to a set of coupled ordinary differential equations for the time dependence of $\mathbf{W}(t)$. However, Eq. (7) holds only if the plasma is a homogeneous ellipsoid *and* the fluid velocity is given by Eq. (6). These two assumptions must be shown to be consistent with one another under the subsequent dynamics described by Eq. (3). Let us consider the motion of the surface of the fluid, assuming that this surface is, at some initial time t, an ellipsoid that satisfies the equation

$$\mathbf{x}\cdot\mathbf{S}^{-2}(t)\cdot\mathbf{x}=1, \tag{8a}$$

where $\mathbf{S}(t)$ is a 3×3 symmetric matrix describing the shape and orientation of the ellipsoid. In body axes, $\mathbf{S}(t)$ takes on a diagonal form

$$\mathbf{S}'(t)=\begin{pmatrix} a_1(t) & & 0 \\ & a_2(t) & \\ 0 & & a_3(t) \end{pmatrix}, \tag{8b}$$

so Eq. (8a) is equivalent to Eq. (2). Since $\nabla\cdot\mathbf{v}=\mathrm{Tr}\,\mathbf{W}$, which is independent of position within the plasma, the velocity field clearly preserves the spatial uniformity of the plasma density. Thus, a short time Δt later, this ellipsoid has changed into a new constant density figure. We must show that this new figure is also an ellipsoid. Since each element on the surface has shifted to a new position $\tilde{\mathbf{x}}$ related to the old position by $\tilde{\mathbf{x}}=\mathbf{x}+\mathbf{W}\cdot\mathbf{x}\Delta t$, the new plasma shape is given by

$$\tilde{\mathbf{x}}\cdot(1-\mathbf{W}^t\Delta t)\cdot\mathbf{S}^{-2}(t)\cdot(1-\mathbf{W}\Delta t)\cdot\tilde{\mathbf{x}}=1,$$

which is clearly the equation for an ellipsoid described by a new tensor

$$\mathbf{S}^{-2}(t+\Delta t)=\mathbf{S}^{-2}(t)-[\mathbf{W}^t\cdot\mathbf{S}^{-2}(t)+\mathbf{S}^{-2}(t)\mathbf{W}]\Delta t$$

(to linear order in Δt). Therefore Eq. (6) is consistent with the assumption that the plasma is a uniform density ellipsoid, and it further follows that the rate of change of the shape of the ellipsoid is determined by

$$\frac{d\mathbf{S}^2}{dt}=\mathbf{W}\cdot\mathbf{S}^2+\mathbf{S}^2\cdot\mathbf{W}^t. \tag{9}$$

Equations (7) and (9) provide a closed self-consistent set of 15 first-order nonlinear differential equations for the nine velocity-related variables in $\mathbf{W}$ and the six independent variables in $\mathbf{S}$. The six variables in $\mathbf{S}$ describe the magnitude of the three principal axes of the ellipsoid together with the orientation of the ellipsoid. We will soon see that the nine variables in the velocity tensor are related to the rates of change of the magnitude of each principal axis, the three components of the rotation frequency of the principal axes, and the three components of the internal vorticity vector describing fluid motions that do not directly alter the shape or orientation of the ellipsoid.

Although the tensor equations (7) and (9) are valid in any inertial frame, in order to make further progress it is useful to explicitly transform the equations to coordinates in which $\mathbf{S}$ is diagonal, i.e., body axes. The transformation to body axes is carried out by the time-dependent unitary rotation matrix $\mathbf{R}$. A vector $\mathbf{x}$ in the lab frame is related to its components $\mathbf{x}'$ in the body frame by $\mathbf{x}'=\mathbf{R}\cdot\mathbf{x}$, and any tensor $\mathbf{T}$ transforms according to $\mathbf{T}'=\mathbf{R}\cdot\mathbf{T}\cdot\mathbf{R}^t$, or equivalently, $\mathbf{T}=\mathbf{R}^t\cdot\mathbf{T}'\cdot\mathbf{R}$. Substitution of the latter relation in Eqs. (7) and (9) leads to the following equations involving components taken with respect to an inertial frame instantaneously aligned with the body axes:

$$\dot{\mathbf{W}}'+\mathbf{W}'\cdot\mathbf{W}'=\omega_z^2\epsilon_e'+\omega_p^2\epsilon_p'+\Omega_c^*\cdot\mathbf{W}'+\boldsymbol{\omega}^*\cdot\mathbf{W}'+\mathbf{W}'\cdot\boldsymbol{\omega}^{*t}, \tag{10}$$

$$\dot{\mathbf{S}}'^2=(\mathbf{W}'+\boldsymbol{\omega}^*)\cdot\mathbf{S}'^2+\mathbf{S}'^2\cdot(\mathbf{W}'^t+\boldsymbol{\omega}^{*t}), \tag{11}$$

where

$$\boldsymbol{\omega}^*\equiv\dot{\mathbf{R}}\cdot\mathbf{R}^t \tag{12}$$

is the rotation frequency matrix. This matrix is antisymmetric since $\mathbf{R}\cdot\mathbf{R}^t=1$ implies $0=(\dot{\mathbf{R}}\cdot\mathbf{R}^t)=\boldsymbol{\omega}^*+\boldsymbol{\omega}^{*t}$. The three independent components of $\boldsymbol{\omega}^*$ are related to the rotation frequency $\boldsymbol{\omega}$ of the body axes through the equation relating an antisymmetric matrix and its dual:

$$\boldsymbol{\omega}^* = -\boldsymbol{\omega}' \times \mathbf{l}, \tag{13}$$

and in this form $\boldsymbol{\omega}^*$ can be recognized as a pseudotensor of rank two. The prime on $\boldsymbol{\omega}$ indicates that components are taken with respect to the body axes. We have also introduced the cyclotron frequency matrix, $\Omega_c^* \equiv -\Omega_c \hat{\mathbf{z}}' \times \mathbf{l}$, in analogy to the definition of $\boldsymbol{\omega}^*$, and we have used the relation $\mathbf{R} \cdot (\hat{\mathbf{z}} \times \mathbf{l}) \cdot \mathbf{R}^t = \hat{\mathbf{z}}' \times \mathbf{l}$, which follows from the transformation properties of pseudotensors under rotations.

Now, Eq. (6) implies that the velocity tensor $\mathbf{W}'$ is related to the fluid velocity $\mathbf{v}'$ as seen in an inertial frame that is instantaneously aligned with the body axes:

$$\mathbf{v}' = \mathbf{W}' \cdot \mathbf{x}'.$$

This inertial fluid velocity is, in turn, related to the noninertial fluid velocity $\mathbf{v}_r$ as seen by an observer moving with the body axes through the transformation $\mathbf{v}_r' = \mathbf{v}' + \boldsymbol{\omega}^* \cdot \mathbf{x}'$. We will now write the equations of motion in this noninertial frame. It is therefore useful to define the matrix $\mathbf{W}_r$:

$$\mathbf{W}_r = \mathbf{W}' + \boldsymbol{\omega}^*, \tag{14}$$

which is the velocity tensor as seen in a noninertial frame rotating with the body axes. In terms of $\mathbf{W}_r$ Eqs. (10) and (11) become

$$\dot{\mathbf{W}}_r - \dot{\boldsymbol{\omega}}^* + \mathbf{W}_r \cdot \mathbf{W}_r = \omega_z^2 \boldsymbol{\epsilon}_e' + \omega_p^2 \boldsymbol{\epsilon}_p' - \boldsymbol{\omega}^* \cdot \boldsymbol{\omega}^* + 2\boldsymbol{\omega}^* \cdot \mathbf{W}_r + \Omega_c^* \cdot \mathbf{W}_r + \Omega_c^* \cdot \boldsymbol{\omega}^{*t}, \tag{15}$$

$$\dot{\mathbf{S}}'^2 = \mathbf{W}_r \cdot \mathbf{S}'^2 + \mathbf{S}'^2 \cdot \mathbf{W}_r^t. \tag{16}$$

The third and fourth terms on the right-hand side of Eq. (15) arise from centrifugal and Coriolis forces appearing in the rotating frame, and the sixth term is due to the extra Lorentz force acting on the rotating body. The first, second, and fifth terms on the right-hand side, respectively, result from the external trap field, the plasma field, and the Lorentz force acting in the fluid motion in the rotating frame.

Note that Eq. (16) for the evolution of the plasma shape takes the same form as in a stationary frame, Eq. (9). However, in the body frame $\mathbf{S}'$ is diagonal, given by Eq. (8b). The diagonal elements of Eq. (16) are $(\partial/\partial t) a_i^2 = 2a_i^2 W_{rii}$. Thus, the diagonal elements of $\mathbf{W}_r$ are simply related to rates of change in the lengths of the principal axes through

$$\dot{a}_i = a_i W_{rii}. \tag{17}$$

Furthermore, Eq. (16) also implies that the off-diagonal elements of $\mathbf{W}_r$ satisfy

$$(\mathbf{W}_r \cdot \mathbf{S}'^2)_{ij} + (\mathbf{W}_r \cdot \mathbf{S}'^2)_{ij}^t = 0, \quad i \neq j$$

so that the off-diagonal elements of $\mathbf{W}_r \cdot \mathbf{S}'^2$ form an antisymmetric matrix that we may write as $\mathbf{S}' \cdot \boldsymbol{\Lambda}^* \cdot \mathbf{S}'$, where $\boldsymbol{\Lambda}^*$ is also an antisymmetric matrix. Together with Eq. (17) this implies that $\mathbf{W}_r$ can be expressed as the sum of a diagonal matrix and a term involving $\boldsymbol{\Lambda}^*$:

$$\mathbf{W}_r = \dot{\mathbf{S}}' \cdot \mathbf{S}'^{-1} + \mathbf{S}' \cdot \boldsymbol{\Lambda}^* \cdot \mathbf{S}'^{-1}. \tag{18}$$

The fluid velocity set up by the second term of Eq. (18) does not change the shape or orientation of the ellipsoid. The three independent components of the matrix $\boldsymbol{\Lambda}^*$ are related to a vector $\boldsymbol{\Lambda}$ that is analogous to the rotation frequency $\boldsymbol{\omega}$:

$$\boldsymbol{\Lambda}^* = -\boldsymbol{\Lambda}' \times \mathbf{l}. \tag{19}$$

We will soon see that this vector $\boldsymbol{\Lambda}$ is the rotation frequency of the fluid plasma with respect to the body axes, and hence the inclusion of this vector in the dynamics allows for the possibility of sheared fluid flow within the ellipsoid. The internal vorticity vector $\boldsymbol{\zeta} \equiv \nabla \times \mathbf{v}_r$ of this internal fluid flow is related to $\boldsymbol{\Lambda}$ by

$$\zeta_i = -\frac{a_j^2 + a_k^2}{a_j a_k} \Lambda_i \quad (i \neq j \neq k), \tag{20}$$

where, as usual, the subscript i refers to components taken along body axes; for example, $\boldsymbol{\Lambda}' = (\Lambda_1, \Lambda_2, \Lambda_3)$.

Equation (18) can be used to reduce Eqs. (15) and (16) to a single-matrix equation for the motion of the ellipsoid. We substitute Eq. (18) into Eq. (15) and act on the right with $\mathbf{S}'$. After some cancellations, we are left with

$$\ddot{\mathbf{S}}' + \frac{d}{dt}(\mathbf{S}' \cdot \boldsymbol{\Lambda}^* - \boldsymbol{\omega}^* \cdot \mathbf{S}') + \dot{\mathbf{S}}' \cdot \boldsymbol{\Lambda}^* - \boldsymbol{\omega}^* \cdot \dot{\mathbf{S}}' + \mathbf{S}' \cdot \boldsymbol{\Lambda}^{*2} + \boldsymbol{\omega}^{*2} \cdot \mathbf{S}' - 2\boldsymbol{\omega}^* \cdot \mathbf{S}' \cdot \boldsymbol{\Lambda}^* = (\omega_z^2 \boldsymbol{\epsilon}_e' + \omega_p^2 \boldsymbol{\epsilon}_p') \cdot \mathbf{S}' + \Omega_c^* \cdot (\dot{\mathbf{S}}' + \mathbf{S}' \cdot \boldsymbol{\Lambda}^* - \boldsymbol{\omega}^* \cdot \mathbf{S}'). \tag{21}$$

These nine equations, together with the three independent equations in Eq. (12), provide a closed set for the variables a_i, ω_i, Λ_i, and the three independent Euler angles that determine $\mathbf{R}$. We have reduced the 15 first-order equations implicit in Eqs. (7) and (9) to a set of three second-order equations and nine first-order equations involving these 12 variables.

Equation (21) closely resembles the force-free equation of motion for a rotating constant density self-gravitating ellipsoidal mass, originally derived by Riemann.[12] However, in that system no external fields are present. If one were to neglect the external fields, one could then show that Eq. (21) is unchanged under the operations of taking the transpose of the equation and interchanging $\boldsymbol{\Lambda}^*$ and $\boldsymbol{\omega}^*$. This implies that external force-free solutions of Eq. (21) come in pairs where $\boldsymbol{\omega}^*$ and $\boldsymbol{\Lambda}^*$ are interchangeable and the ellipsoid shape is the same in both cases. This symmetry is known as Dedekind's theorem in the astrophysics literature.[12] However, the symmetry is clearly broken when external fields are added.

On the other hand, a less general symmetry in the dynamics can be uncovered if we introduce the vortex frequency matrix $\Omega_v^* \equiv \Omega_c^* + 2\boldsymbol{\omega}^*$. The vortex frequency vector Ω_v is related to Ω_v^* through equations analogous to Eq. (13): $\Omega_v^* = -\Omega_v' \times \mathbf{l}$, which implies $\Omega_v = \Omega_c + 2\boldsymbol{\omega}$. The vortex frequency is the cyclotron frequency as seen in a noninertial frame rotating with frequency $\boldsymbol{\omega}$.[15] Substituting

for ω^* in terms of Ω_v^* in Eq. (21) we obtain, after some cancellations, an equivalent form for the equation of motion:

$$\ddot{\mathbf{S}}'+2\dot{\mathbf{S}}'\cdot\mathbf{\Lambda}^*+\mathbf{S}'\cdot\dot{\mathbf{\Lambda}}^*-\tfrac{1}{2}\dot{\Omega}_v^*\cdot\mathbf{S}'-\Omega_v^*\cdot\dot{\mathbf{S}}'+\mathbf{S}'\cdot\mathbf{\Lambda}^{*2}$$
$$+\tfrac{1}{4}(\Omega_v^*-\Omega_c^*)\cdot(\Omega_v^*+\Omega_c^*)\cdot\mathbf{S}'-\Omega_v^*\cdot\mathbf{S}'\cdot\mathbf{\Lambda}^*$$
$$-(\omega_z^2\epsilon_e'+\omega_p^2\epsilon_p')\cdot\mathbf{S}'=0. \tag{22}$$

This equation is invariant under the transformation $\Omega_v^* \rightarrow -\Omega_v^*$, $\mathbf{\Lambda}^*\rightarrow-\mathbf{\Lambda}^*$, $t\rightarrow -t$, if and only if Ω_v^* and Ω_c^* commute. Thus, if (and only if) $\boldsymbol{\omega}$ and Ω_c are parallel, the solutions of Eq. (22) occur in pairs in which the ellipsoid has the same shape but Ω_v and $\mathbf{\Lambda}$ have opposite signs. We will return to this symmetry in the next section, where we will find that it applies to the equilibrium solutions of Eq. (22).

The components of Eq. (22) can be expressed in a fairly simple form for the case of the cylindrically symmetric external trap field, given by Eqs. (4). In order to explicitly parametrize the rotation of the external trap field and magnetic field as seen in body axes, we employ the Euler angles (ϕ,θ,ψ) (see Fig. 1). In terms of these angles, the rotation matrix $\mathbf{R}$ takes on the well-known form[16]

$$\mathbf{R}=\begin{pmatrix} \cos\psi\cos\phi-\cos\theta\sin\phi\sin\psi & \cos\psi\sin\phi+\cos\theta\cos\phi\sin\psi & \sin\psi\sin\theta \\ -\sin\psi\cos\phi-\cos\theta\sin\phi\cos\psi & -\sin\psi\sin\phi+\cos\theta\cos\phi\cos\psi & \cos\psi\sin\theta \\ \sin\theta\sin\phi & -\sin\theta\cos\phi & \cos\theta \end{pmatrix}. \tag{23}$$

It then turns out that the components of Eq. (22) depend on the Euler angles only through the components (z_1,z_2,z_3) of the laboratory z unit vector along the body axes; these components are

$$\hat{\mathbf{z}}'=\mathbf{R}\cdot\hat{\mathbf{z}}=(\sin\theta\sin\psi,\sin\theta\cos\psi,\cos\theta)\equiv(z_1,z_2,z_3).$$

The components of Eq. (22) depend on the Euler angles only through (z_1,z_2,z_3) because $\hat{\mathbf{z}}$ is the mutual axis of symmetry of the external cylindrically symmetric electric and magnetic fields, so it is the only unit vector on which the rotation of these fields can depend. The diagonal elements of Eq. (22) are

$$\ddot{a}_i-a_i\left(\frac{1}{2}\omega_z^2(1-3z_i^2)+\frac{1}{2}\omega_p^2A_i+\sum_{k\neq i}[\omega_k(\Omega_cz_k+\omega_k)+\Lambda_k^2]\right)$$
$$+\sum_{j\neq k\neq i}a_j\Lambda_k\Omega_{v_k}=0, \tag{24a}$$

The off-diagonal elements of Eq. (22) have a different form:

$$\sum_{k=1}^{3}\epsilon_{ijk}(2\dot{a}_i\Lambda_k-\dot{a}_j\Omega_{v_k}+a_i\dot{\Lambda}_k-a_j\dot{\omega}_k-\epsilon_{ijk}\Lambda_i\Omega_{v_j}a_k)$$
$$+a_i\Lambda_i\Lambda_j+a_j\omega_j(\Omega_cz_i+\omega_i)+\frac{3}{2}a_j\omega_z^2z_iz_j=0 \quad (i\neq j), \tag{24b}$$

where ϵ_{ijk} is a Levi-Civita symbol.

Finally, Eq. (12) can be used together with Eq. (23) to obtain the well-known relations between the Euler angles and components of $\boldsymbol{\omega}$ along body axes:

$$\omega_1=\dot{\phi}\sin\theta\sin\psi+\dot{\theta}\cos\psi,$$
$$\omega_2=\dot{\phi}\sin\theta\cos\psi-\dot{\theta}\sin\psi, \tag{24c}$$
$$\omega_3=\dot{\phi}\cos\theta+\dot{\psi}.$$

Equations (24) provide a closed set of 12 coupled differential equations for the 12 variables a_i, (ϕ,θ,ψ), $\boldsymbol{\omega}$, and $\mathbf{\Lambda}$. The first three variables describe the shape of the ellipsoid, the second three describe the orientation of the ellipsoid with respect to the laboratory reference frame, the next three describe the rate of change of this orientation and the last three describe the motion of the fluid with respect to the body axes due to fluid flow within the ellipsoid.

B. Integrals of the motion

Equations (24) admit several conserved quantities, which are most readily uncovered by considering the fluid motion in a Hamiltonian framework. We begin by writing down the Lagrangian for N charges moving in a self-consistent electrostatic potential and a uniform magnetic field:[17]

$$\mathscr{L}=\sum_{i=1}^{N}\left(\frac{1}{2}m\mathbf{v}_i^2+\frac{q}{c}\mathscr{A}(\mathbf{x})\cdot\mathbf{v}_i-\frac{1}{2}q\phi_p(\mathbf{x}_i)-q\phi_e(\mathbf{x}_i)\right),$$

where ϕ_e is the externally applied electrostatic potential, $\phi_p=\Sigma_{j\neq i}q/|\mathbf{x}_i-\mathbf{x}_j|$ is the space-charge potential at $\mathbf{x}_i$ induced by all the other charges, and $\mathscr{A}$ is the magnetic vector potential, equal to $(q/2c)B(x\hat{\mathbf{y}}-y\hat{\mathbf{x}})$ for a cylindrically symmetric system. This general Lagrangian has a large number $(3N)$ of degrees of freedom. However, when we specialize to the motion of a homogeneous ellipsoid, $\mathscr{L}$ simplifies considerably. We obtain a fluid Lagrangian by replacing sums over the particles by integrals over the fluid density, also replacing the particle velocity by the fluid velocity. Then using Eqs. (A2), (A3), (1), and (6), together with the relations $\int n\,d^3x=N$ and $\int nx_ix_j\,d^3x=N(\mathbf{S}^2)_{ij}/5$ [which follows from Eq. (8)], we obtain

$$\mathscr{L}=(mN/10)\mathrm{Tr}[\mathbf{S}^2\cdot(\mathbf{W}^t\cdot\mathbf{W}-\Omega_c\hat{\mathbf{z}}\times\mathbf{W}-2\omega_p^2\epsilon_p-\omega_z^2\epsilon_e)].$$

Since the trace is invariant under rotations, $\mathscr{L}$ has the same form in an inertial frame instantaneously oriented with the body axes (where all vectors and tensors are primed). To make further progress, we express $\mathscr{L}$ in terms of $\dot{a}_j$, $\mathbf{\Lambda}$, and $\boldsymbol{\omega}$ using Eqs. (4b), (5b), (8b), (13), (14), (18), and (19). We write the result in terms of a sum of the kinetic, potential, and magnetic contributions to $\mathscr{L}$:

$$\mathscr{L}=\mathscr{K}+\mathscr{M}-\mathscr{P}, \tag{25a}$$

where the kinetic energy $\mathscr{K}$ is

$$\mathscr{K}=\frac{mN}{10}\sum_i\left[\dot{a}_i^2+(a_j^2+a_k^2)(\Lambda_i^2+\omega_i^2)-4a_ja_k\Lambda_i\omega_i\right]$$

$$(i\neq j\neq k), \tag{25b}$$

the potential energy $\mathscr{P}$ is a sum of the plasma potential and external field energies:

$$\mathscr{P}=\frac{mN}{10}\omega_p^2\sum_i A_ia_i^2-\frac{mN}{20}\omega_z^2\sum_i a_i^2(1-3z_i^2), \tag{25c}$$

and the magnetic term $\mathscr{M}$ is

$$\mathscr{M}=\frac{mN\Omega_c}{10}\sum_i z_i[\omega_i(a_j^2+a_k^2)-2\Lambda_ia_ja_k]\quad(i\neq j\neq k). \tag{25d}$$

It may be easily verified that the Lagrange variational equations for a_i lead directly to Eq. (24a), provided that we employ Eq. (A9), as well as the relationship between the plasma frequency and volume V of the ellipsoid. That is, since $V=4\pi a_1a_2a_3/3$ the plasma frequency is a function of the lengths of the principal axes:

$$\omega_p^2=3q^2N/(ma_1a_2a_3)\,, \tag{26}$$

and this relation must be employed when derivatives of $\mathscr{L}$ with respect to the a_i's are taken. We also find that the momenta conjugate to the $\dot{a}_i$'s are

$$p_{a_i}=\frac{\partial\mathscr{L}}{\partial\dot{a}_i}=\frac{mN\dot{a}_i}{5},$$

so one can associate an inertial mass $mN/5$ with changes in the lengths of the body axes.

Turning to the Lagrange variational equations for the Euler angles (θ,ϕ,ψ), we must first express $\boldsymbol{\omega}$ in terms of $(\dot{\phi},\dot{\theta},\dot{\psi})$ through Eq. (24c). It is then clear from these equations and from Eqs. (25) that $\mathscr{L}$ is independent of ϕ, so that the momentum conjugate to this angle is a conserved quantity:

$$p_\phi=\frac{\partial\mathscr{L}}{\partial\dot{\phi}}=\text{const.}$$

Furthermore, with the aid of Eqs. (25) and (24c), $\partial\mathscr{L}/\partial\dot{\phi}$ can be determined explicitly in terms of the z component of the canonical angular momentum, $\mathbf{L}$:

$$p_\phi=\mathbf{L}\cdot z=\mathbf{L}'\cdot\hat{\mathbf{z}}', \tag{27a}$$

where $\mathbf{L}'\equiv(L_1,L_2,L_3)$ refers to components of $\mathbf{L}$ in body axes, which take on a simple form in terms of $\mathbf{\Lambda}$ and $\Omega_{\mathbf{v}}$:

$$L_i=(mN/10)\left[(a_j^2+a_k^2)\Omega_{\mathbf{v}i}-4a_ja_k\Lambda_i\right]\quad(i\neq j\neq k), \tag{27b}$$

and the components of $\hat{\mathbf{z}}'$ were given previously [see the discussion following Eqs. (23)]. Of course, the invariance of p_ϕ depends on our choice of a cylindrically symmetric form of the external trap field, which we reiterate is not a required assumption in the ellipsoidal dynamics described by Eq. (22). We also note that Eq. (27) could also have been obtained directly from the form of the canonical angular momentum for a magnetized fluid:

$$\mathbf{L}\cdot\hat{\mathbf{z}}=\int d^3x\,n(\mathbf{x},t)\left(m(v_yx-v_xy)+\frac{q}{c}(\mathscr{A}_yx-\mathscr{A}_xy)\right).$$

There are several more integral invariants of Eq. (24) that are perhaps not as obvious, but that are reasonably easy to derive using the Lagrangian. In order to find these invariants, we observe that there are three variables that were not required in Eqs. (24), but that are required in the Lagrangian picture in order to form a complete set of degrees of freedom and their time derivatives. These extra variables involve the internal motions of the fluid, and become apparent if we recognize that $\mathbf{\Lambda}^*$, in analogy to $\boldsymbol{\omega}^*$, can be written in terms of the time derivative of a unitary time-dependent rotation matrix that we call $\mathbf{F}$:

$$\mathbf{\Lambda}^*=\dot{\mathbf{F}}\cdot\mathbf{F}^t. \tag{28}$$

The matrix $\mathbf{F}$ describes rotational motion of a fluid element in the ellipsoid with respect to the body axes. This follows from Eq. (18), together with the equation of motion for the position $\mathbf{x}'(t)$ of a fluid element with respect to the body axes:

$$\frac{d\mathbf{x}'}{dt}=\mathbf{W}_r\cdot\mathbf{x}'.$$

If we then substitute for $\mathbf{W}_r$ via Eq. (18), act on the left with $\mathbf{S}^{-1}$, and employ Eq. (28), we obtain

$$\frac{d}{dt}(\mathbf{S}^{-1}\cdot\mathbf{x}')=\dot{\mathbf{F}}\cdot\mathbf{F}^t\cdot\mathbf{S}^{-1}\cdot\mathbf{x}'.$$

Finally, this equation can be solved if we employ the relation $(d/dt)(\mathbf{F}\cdot\mathbf{F}^t)=0$, and the result is

$$\mathbf{S}^{-1}(t)\cdot\mathbf{x}'(t)=\mathbf{F}(t)\cdot\mathbf{S}^{-1}(0)\cdot\mathbf{x}'(0), \tag{29}$$

where the initial condition $\mathbf{F}(0)=1$ has been used. Equation (29) implies that the internal fluid motions of the ellipsoid, as seen in the body frame, consist of expansions and compressions described by $\mathbf{S}(t)$, together with motions described by $\mathbf{F}(t)$, which are purely rotational (provided that we scale out the compressions and expansions with $\mathbf{S}^{-1}$).

The three independent components of $\mathbf{F}$ can be described by three new internal fluid Euler angles (ϕ_f,θ_f,ψ_f), in analogy to Eq. (23), that serve as the three extra variables that were not required in the previous description of the motion, Eq. (24). [The fact that they were not required in Eq. (24) in itself points to the existence of hidden invariants.] These fluid Euler angles determine the orientation of a fluid element with respect to the body axes, just as

the usual Euler angles determine the orientation of the body axes with respect to the laboratory frame. Only three fluid Euler angles are required to describe the orientation of any fluid element in the plasma because of the particularly simple linear velocity field assumed in Eq. (6). The initial condition $\mathbf{F}(0)=1$ implies the fluid Euler angles are initially zero. In other words, we can define three new unit vectors $(\hat{\mathbf{e}}_{f1},\hat{\mathbf{e}}_{f2},\hat{\mathbf{e}}_{f3})$, which describe orthogonal axes fixed in the fluid and which are initially oriented along the principal axes. The subsequent direction of these axes is related to the fluid Euler angles. For example, the unit vector $\hat{\mathbf{e}}_{f3}$ has components as seen in the body frame that vary in time according to

$$\hat{\mathbf{e}}'_{f3}=\mathbf{F}\cdot(0,0,1)=(\sin\theta_f\sin\psi_f,\sin\theta_f\cos\psi_f,\cos\theta_f).$$

Equation (28) provides a set of relations, analogous to Eq. (24c), linking components of $\mathbf{\Lambda}$ to time derivatives of the fluid Euler angles:

$$\begin{aligned}\Lambda_1&=\dot{\phi}_f\sin\theta_f\sin\psi_f+\dot{\theta}_f\cos\psi_f,\\ \Lambda_2&=\dot{\phi}_f\sin\theta_f\cos\psi_f-\dot{\theta}_f\sin\psi_f,\\ \Lambda_3&=\dot{\phi}_f\cos\theta_f+\dot{\psi}_f.\end{aligned}\tag{30}$$

When these equations are substituted into Eq. (25) we see immediately that the Lagrangian is independent of ϕ_f, the angle by which the fluid has rotated around the three-body axis. The momentum p_{ϕ_f} conjugate to ϕ_f is therefore a constant of the motion, and is given by

$$p_{\phi_f}=\frac{\partial\mathscr{L}}{\partial\dot{\phi}_f}=\text{const.}$$

Unlike the conservation of p_ϕ, this result is independent of the external field symmetry, resting instead upon the assumption that the fluid motion conserves entropy.[11]

The derivative $\partial\mathscr{L}/\partial\dot{\phi}_f$ can, after some effort, be written as the component of the canonical circulation vector $\mathbf{C}$ along the direction $\hat{\mathbf{e}}_{f3}$:

$$p_{\phi_f}=\mathbf{C}\cdot\hat{\mathbf{e}}_{f3}=\mathbf{C}'\cdot\hat{\mathbf{e}}'_{f3},\tag{31a}$$

where, as usual, the prime refers to components taken in inertial axes instantaneously aligned with the body axes. The components of $\mathbf{C}'$ are

$$C_i=(Nm/5)(\zeta_i+\Omega_{v_i})a_ja_k\quad(i\neq j\neq k).\tag{31b}$$

The vector $\mathbf{C}$ is referred to as the canonical circulation vector because the conservation of p_{ϕ_f} is equivalent to the conservation of canonical circulation for an ideal fluid:[11]

$$\int\left[\nabla\times\left[\mathbf{v}+\left(\frac{q}{mc}\right)\mathscr{A}\right]\right]\cdot d\mathbf{S}=\int(\zeta+\Omega_v)\cdot d\mathbf{S}=\text{const},$$

where the integral is taken over any area element $d\mathbf{S}$ which moves with the fluid. In the case of Eq. (31a) $\hat{\mathbf{e}}_{f3}$ is normal to the area element. However, since the choice of the direction of the $\hat{\mathbf{e}}_{f3}$ axis was arbitrary, any component of $\mathbf{C}$ taken along an axis moving with the fluid is constant, so there are in fact three independent constants of the motion involving the angles (ϕ_f,θ_f,ψ_f):

$$\begin{aligned}\mathbf{C}\cdot\hat{\mathbf{e}}_{f1}&=\text{const},\\ \mathbf{C}\cdot\hat{\mathbf{e}}_{f2}&=\text{const},\\ \mathbf{C}\cdot\hat{\mathbf{e}}_{f3}&=\text{const}.\end{aligned}\tag{32}$$

In other words, $\mathbf{C}$ is fixed in a frame moving with the internal motions of the fluid [including the compressions and expansions that rescale the frame according to Eq. (29)].

However, it is clear from the form of the Lagrangian that the equations of motion for a_i and (θ,ϕ,ψ) depend on (ϕ_f,θ_f,ψ_f) only through $\mathbf{\Lambda}$ [this also follows from Eq. (22) or Eq. (24)], and so the equations of motion can be integrated without reference to these angles. It is therefore useful to identify those combinations of the constants that are independent of (ϕ_f,θ_f,ψ_f). The only such combination is

$$C^2=C_1^2+C_2^2+C_3^2=\text{const}.\tag{33}$$

Finally, the last invariant hidden in Eq. (22) is clearly the total energy

$$\mathscr{H}=\mathscr{K}+\mathscr{P}.\tag{34}$$

In summary, Eq. (25) is the Lagrangian for the motion of the ellipsoid, which has nine degrees of freedom: $(a_1,a_2,a_3,\phi,\theta,\psi,\phi_f,\theta_f,\psi_f)$. The first three degrees of freedom describe the shape of the ellipsoid; the second three describe the orientation of the ellipsoid, and the last three describe internal rotations of the fluid with respect to the body axes. The rotation frequency of the body axes is $\boldsymbol{\omega}$, and the rotation frequency of the internal fluid motions is $\mathbf{\Lambda}$. Equation (34) is the Hamiltonian (Jacobi integral) for this system. It, along with the canonical circulation $\mathbf{C}$ and the z component of the angular momentum $\mathbf{L}\cdot\hat{\mathbf{z}}$ are conserved during the motion. However, the number of constants is not sufficient to reduce the system to quadratures, so the system is not integrable, and may display complicated chaotic behavior.

Equations (24) are in a form suitable for numerical integration of the system. The constants $\mathscr{H}$, $\mathbf{L}\cdot\hat{\mathbf{z}}$, and $\mathbf{C}^2$ can be employed to further reduce the number of variables, or can be used to check the accuracy of the numerics.

However, there are special initial conditions for which the motion simplifies considerably. We consider these in the next subsection.

C. Simplified dynamics for special initial conditions

Let us consider a subset of the possible motions described by Eq. (24), for which the initial conditions satisfy $\omega_1=\omega_2=\Lambda_1=\Lambda_2=\theta=0$. We will see that, for these initial conditions, the ellipsoid always remains oriented with a principal axis aligned along $\hat{\mathbf{z}}$, and in this case the equations of motion simplify. In fact, the (1,3), (3,1), (2,3), and (3,2) components of Eq. (24b) imply that $\dot{\Lambda}_1=\dot{\Lambda}_2=\dot{\omega}_1=\dot{\omega}_2=0$, and Eqs. (24c) imply $\dot{\theta}=0$ as well. We are then left with Eq. (24a) and the (1,2) and (2,1) elements of Eq. (24b).

We write these equations in terms of dimensionless variables $\bar{\omega}=\omega/\omega_z$, $\bar{\Omega}_c=\Omega_c/\omega_z$, $\bar{\Omega}_v=\Omega_v/\omega_z$ and $\bar{\Lambda}=\Lambda/\omega_z$, and we normalize times to ω_z: $\bar{t}=t\omega_z$. We also introduce dimensionless variables $\bar{a}_i=a_i/a_0$, where a_0 is defined in order to take account of the dependence of ω_p^2 on the a_i's: $a_0\equiv(3Nq^2/m\omega_z^2)^{1/3}$ [see Eq. (26)]. This length scale has a simple physical interpretation: $a_0/3^{1/3}$ is the radius that a uniform density N particle plasma takes on when it is spherically symmetric and in equilibrium in the trap. The introduction of a_0 allows us to scale out the overall size of the plasma (i.e., the dependence of the plasma frequency on the total number of particles in the plasma). We could have introduced this scaling in the previous section but we preferred to work with dimensional equations. In this section, however, we will examine numerical solutions of the equations so dimensionless variables are required. In these variables, the solutions depend, for given initial conditions, on a single parameter $\bar{\Omega}_c$ which determines the relative magnitude of the external magnetic and electrostatic trap fields.

In these dimensionless variables, the diagonal elements are obtained from Eq. (24a):

$$\ddot{\bar{a}}_1-\bar{a}_1[\tfrac{1}{2}+A_1/(2\bar{a}_1\bar{a}_2\bar{a}_3)+\bar{\omega}(\bar{\Omega}_c+\bar{\omega})+\bar{\Lambda}^2]+\bar{a}_2\bar{\Lambda}\bar{\Omega}_v=0, \tag{35a}$$

$$\ddot{\bar{a}}_2-\bar{a}_2[\tfrac{1}{2}+A_2/(2\bar{a}_1\bar{a}_2\bar{a}_3)+\bar{\omega}(\bar{\Omega}_c+\bar{\omega})+\bar{\Lambda}^2]+\bar{a}_1\bar{\Lambda}\bar{\Omega}_v=0, \tag{35b}$$

$$\ddot{\bar{a}}_3-\bar{a}_3[-1+A_3/(2\bar{a}_1\bar{a}_2\bar{a}_3)]=0, \tag{35c}$$

where we have dropped the body axis subscript 3 from $\bar{\omega}_3$ and $\bar{\Lambda}_3$ for convenience. The (1,2) and (2,1) components of Eqs. (24b) are

$$2\dot{\bar{a}}_1\bar{\Lambda}-\dot{\bar{a}}_2\bar{\Omega}_v+\bar{a}_1\dot{\bar{\Lambda}}-\bar{a}_2\dot{\bar{\omega}}=0, \tag{36a}$$

$$-2\dot{\bar{a}}_2\bar{\Lambda}+\dot{\bar{a}}_1\bar{\Omega}_v-\bar{a}_2\dot{\bar{\Lambda}}+\bar{a}_2\dot{\bar{\omega}}=0. \tag{36b}$$

However, these last equations are merely expressions of the conservation of p_ϕ and p_{ϕ_f}. For example, the equation $(a_1^2+a_2^2)\dot{p}_\phi-4a_1a_2\dot{p}_{\phi_f}=0$ can be written with the aid of Eqs. (27) and (31) as

$$(a_1^2-a_2^2)[2\dot{\omega}(a_1^2-a_2^2)+2(a_1\dot{a}_1-a_2\dot{a}_2)\Omega_v+4(a_2\dot{a}_1-a_1\dot{a}_2)\Lambda]=0,$$

which is identical to Eq. (36a) multiplied by a_2 minus Eq. (36b) multiplied by a_1 [except for a factor of $2(a_1^2-a_2^2)$]. In fact, we can determine $\bar{\omega}$ and $\bar{\Lambda}$ in terms of p_ϕ and p_{ϕ_f}:

$$\bar{\omega}=\frac{(\bar{a}_1^2+\bar{a}_2^2)\bar{p}_\phi-2\bar{a}_1\bar{a}_2\bar{p}_{\phi_f}}{(a_1^2-a_2^2)^2}-\frac{\bar{\Omega}_c}{2},$$
$$\bar{\Lambda}=-\frac{(\bar{a}_1^2+\bar{a}_2^2)\bar{p}_{\phi_f}-2\bar{a}_1\bar{a}_2\bar{p}_\phi}{(a_1^2-a_2^2)^2}, \tag{37}$$

where $\bar{p}_\phi$ and $\bar{p}_{\phi_f}$ are normalized by $Nma_0^2\omega_z^2/5$.

When Eqs. (37) are substituted into Eqs. (35), we obtain three coupled equations with three degrees of freedom, $(\bar{a}_1,\bar{a}_2,\bar{a}_3)$, which can be most economically expressed in terms of the combinations

$$K_1=\bar{p}_\phi+\bar{p}_{\phi_f},$$
$$K_2=\bar{p}_\phi-\bar{p}_{\phi_f}. \tag{38}$$

The equations are

$$\ddot{\bar{a}}_1-\bar{a}_1\left(\frac{1}{2}+\frac{A_1}{2\bar{a}_1\bar{a}_2\bar{a}_3}-\frac{1}{4}\bar{\Omega}_c^2\right)-\frac{1}{2}\frac{K_2^2}{(\bar{a}_1-\bar{a}_2)^3}-\frac{1}{2}\frac{K_1^2}{(\bar{a}_1+\bar{a}_2)^3}=0,$$
$$\ddot{\bar{a}}_2-\bar{a}_2\left(\frac{1}{2}+\frac{A_2}{2\bar{a}_1\bar{a}_2\bar{a}_3}-\frac{1}{4}\bar{\Omega}_c^2\right)-\frac{1}{2}\frac{K_2^2}{(\bar{a}_2-\bar{a}_1)^3}-\frac{1}{2}\frac{K_1^2}{(\bar{a}_1+\bar{a}_2)^3}=0, \tag{39}$$
$$\ddot{\bar{a}}_3-\bar{a}_3\left(-1+\frac{A_3}{2\bar{a}_1\bar{a}_2\bar{a}_3}\right)=0.$$

These equations have a Hamiltonian that can be found by substituting Eqs. (37) and (38) into Eq. (34):

$$\bar{\mathscr{H}}=\frac{1}{2}\left(\sum_i\bar{p}_{a_i}^2+\frac{1}{2}\frac{K_1^2}{(\bar{a}_1+\bar{a}_2)^2}+\frac{1}{2}\frac{K_2^2}{(\bar{a}_1-\bar{a}_2)^2}-\frac{1}{2}(K_1+K_2)\bar{\Omega}_c+\frac{1}{4}(\bar{a}_1^2+\bar{a}_2^2)\bar{\Omega}_c^2+\sum_i\frac{A_i\bar{a}_i^2}{\bar{a}_1\bar{a}_2\bar{a}_3}+\bar{a}_3^2-\frac{1}{2}(\bar{a}_1^2+\bar{a}_2^2)\right), \tag{40}$$

where $\bar{p}_{a_i}=\dot{\bar{a}}_i$ is the momentum conjugate to $\bar{a}_i$, and $\bar{\mathscr{H}}\equiv\mathscr{H}/(Nm\omega_z^2a_0^2/5)$.

The motions described by Eqs. (39) and (40) are coupled nonlinear oscillations in the lengths of the principal axes with a single constant of the motion, $\bar{\mathscr{H}}$. The motion is therefore not integrable in general. Furthermore, the form of the effective potential in $\bar{\mathscr{H}}$ has a singularity at $a_1=a_2$, so that $a_1=a_2$ is inaccessible to the dynamics unless $K_2=0$.

If this is the case, we can then simplify further and consider initial conditions where $a_1=a_2$ and $\dot{a}_1=\dot{a}_2$, so that the motion remains spheroidal for all times. This is a finite-amplitude version of the (2,0) linear normal mode of oscillation.[5–7] The equations of motion are now

$$\ddot{\bar{a}}_1-\bar{a}_1\left(\frac{1}{2}+\frac{A_1}{2\bar{a}_1^2\bar{a}_3}-\frac{1}{4}\bar{\Omega}_c^2\right)-\frac{1}{16}\frac{K_1^2}{\bar{a}_1^3}=0, \tag{41a}$$

$$\ddot{\bar{a}}_3-\bar{a}_3\left(-1+\frac{A_3}{2\bar{a}_1^2\bar{a}_3}\right)=0, \tag{41b}$$

with an effective spheroidal Hamiltonian $\bar{\mathscr{H}}_s$, where

$$\bar{\mathscr{H}}_s=\frac{1}{2}\left(\frac{1}{2}\bar{p}_r^2+\bar{p}_{a_3}^2+\frac{1}{8}\frac{K_1^2}{\bar{a}_1^2}-\frac{K_1}{2}\bar{\Omega}_c+\frac{\bar{a}_1^2}{2}\bar{\Omega}_c^2+\frac{2A_1\bar{a}_1^2+A_3\bar{a}_3^2}{\bar{a}_1^2\bar{a}_3}+\bar{a}_3^2-\bar{a}_1^2\right), \tag{42}$$

and where $\bar{p}_r$ is the radial momentum, canonically conjugate to $\bar{a}_1$ and equal to $2\dot{\bar{a}}_1$. Equations (41) and (42) describe two coupled nonlinear oscillations in the radius and length of the spheroid. Note that Eqs. (38) imply that K_1 is equal to twice the canonical angular momentum, so the appearance in Eq. (42) of the centrifugal potential $K_1^2/8\bar{a}_1^2$ is not surprising. Again, the system is not integrable in general since there are two degrees of freedom but only a single constant of the motion, $\mathscr{H}_s$.

The equilibria of Eq. (41) satisfy the relations

$$-\bar{a}_1\left(\frac{1}{2}+\frac{A_1(a_3/a_1)}{2\bar{a}_1^2\bar{a}_3}-\frac{1}{4}\bar{\Omega}_c^2\right)-\frac{1}{16}\frac{K_1^2}{\bar{a}_1^3}=0 \tag{43a}$$

and

$$\frac{A_3(a_3/a_1)}{2\bar{a}_1^2\bar{a}_3}-1=0. \tag{43b}$$

Equations (43) are simply expressions of force balance in the radial and axial directions. If we consider Eq. (43b) as an equation for $\bar{a}_3$ and substitute the solution into Eq. (43a), and if we further substitute for $K_1=2\bar{p}_\phi$ in terms of $\bar{\omega}$ and $\bar{\Lambda}$ using Eq. (27), we find that Eq. (43a) becomes

$$-(\bar{\omega}-\bar{\Lambda})(\bar{\Omega}_c+\bar{\omega}-\bar{\Lambda})-\frac{1}{2}=\frac{A_1(a_3/a_1)}{A_3(a_3/a_1)}, \tag{44}$$

where $\bar{\omega}-\bar{\Lambda}$ is just the total rigid rotation frequency of the fluid around the z axis. This equation is actually the well-known relation between the rotation frequency and shape of a rigid-rotor equilibrium spheroid.[1] We will consider more general equilibria of Eqs. (24) in the next section.

Furthermore, one can easily show that, if one linearizes Eqs. (41) around the equilibrium given by Eq. (43), one recovers the linear dispersion relation of the two (2,0) normal modes of Refs. 5–7. This simple calculation is left to the reader. As we discussed in the Introduction, for large $\bar{\Omega}_c$ these modes are a plasma oscillation in which the spheroid expands and contracts mainly along the magnetic field, and an upper-hybrid oscillation at a frequency near Ω_c, in which the spheroid expands and contracts primarily across the magnetic field.

Equations (41) have been integrated numerically for various initial conditions. Some results are shown in Fig. 3. Nonlinear coupling between the upper-hybrid and plasma oscillations is clearly observable. A Poincaré plot of the motions is included in Fig. 4, which graphically shows that stochastic orbits can occur. From this fact, we can infer that the integral invariants discussed in Sec. II B are the only invariants, since the existence of one more independent invariant would make this two-degree-of-freedom system integrable. However, in the limit of large $\bar{\Omega}_c$ the system is nearly integrable. We can see directly from Eqs. (41) that, for large $\bar{\Omega}_c$, the radial oscillations are at much higher frequency than the axial oscillations. This suggests that a two-time-scale approach may be useful in analyzing the equations. We note from Eqs. (27), (31), and (38) that $K_1=2\bar{a}_1^2[\bar{\Omega}_c+2(\bar{\omega}-\bar{\Lambda})]$ when $\bar{a}_1=\bar{a}_2$, and so $\bar{a}_1$ is almost constant for large $\bar{\Omega}_c$. This is just the guiding-center limit

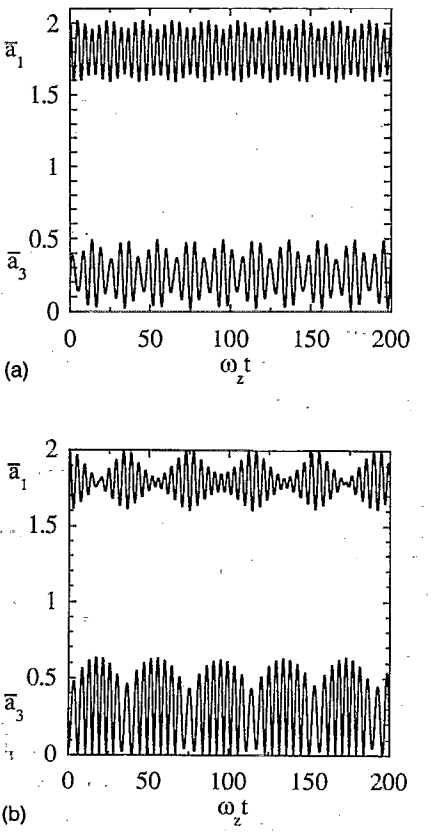

FIG. 3. Numerical solutions of Eqs. (41) for the oscillations in radius and length of a homogeneous plasma spheroid. Upper curve is plasma radius $\bar{a}_1$ versus time, lower curve is plasma length/2 $\bar{a}_3$ versus time. (a) $\bar{\Omega}_c=2$, $K_1=8$, $\dot{\bar{a}}_1(0)=0$, $\dot{\bar{a}}_3=0.1714$, $\bar{a}_1(0)=2$, $\bar{a}_3(0)=0.25$. (b) $\bar{\Omega}_c=2$, $K_1=8$, $\dot{\bar{a}}_1(0)=0=\dot{\bar{a}}_3(0)$, $\bar{a}_1(0)=2$, $\bar{a}_3(0)=0.05$. These two orbits are chosen to have the same energy and angular momentum, so that they can be displayed on the same Poincaré plot (Fig. 4).

of the dynamics, in which mean-square cylindrical radius of the plasma is a conserved quantity.[18] We therefore take $\bar{a}_1(t)$ equal to its initial value $\bar{a}_1(0)$ in Eq. (41b), in which case the motion of $\bar{a}_3$ is integrable, given by the integral

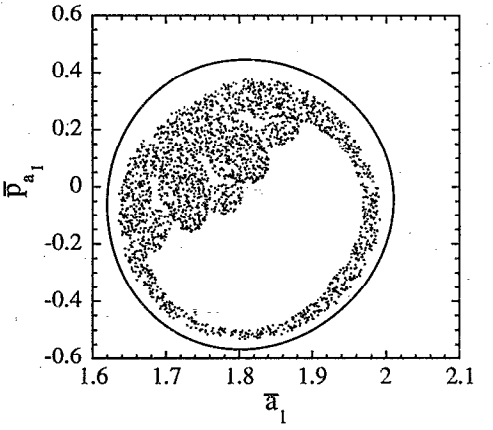

FIG. 4. Poincaré surface of section for motions corresponding to Figs. 3(a) and 3(b). Each point occurs at $a_3=0.2$, $\dot{a}_3>0$. The stochastic orbit corresponds to Fig. 3(b), whereas the integrable orbit corresponds to Fig. 3(a).

$$\int^{\bar{a}_3(t)} \frac{d\bar{a}_3}{\sqrt{2\bar{\mathscr{H}}_\parallel - 2\phi_{\rm eff}(\bar{a}_3,\bar{a}_1)}} = \bar{t}, \tag{45a}$$

where $\bar{a}_1$ is understood to be constant, $\phi_{\rm eff}$ is the effective potential of the $\bar{a}_3$ motion:

$$\phi_{\rm eff}(\bar{a}_3,\bar{a}_1) = \frac{1}{2}\left(\frac{(2A_1\bar{a}_1^2 + A_3\bar{a}_3^2)}{\bar{a}_1^2\bar{a}_3} + \bar{a}_3^2\right), \tag{45b}$$

and where $A_i = A_i(a_3/a_1)$, and $\bar{\mathscr{H}}_\parallel$ is the constant energy of these nonlinear plasma oscillations:

$$\bar{\mathscr{H}}_\parallel = \frac{1}{2}\dot{\bar{a}}_3^2 + \phi_{\rm eff}. \tag{46}$$

As usual, the branch of the square root in Eq. (45a) changes sign at the upper and lower turning points $\bar{a}_3^{(1)}(\bar{\mathscr{H}}_\parallel, \bar{a}_1)$ and $\bar{a}_3^{(2)}(\bar{\mathscr{H}}_\parallel, \bar{a}_1)$, which are determined by solutions of $\bar{\mathscr{H}}_\parallel = \phi_{\rm eff}(\bar{a}_3^{(1,2)}, \bar{a}_1)$.

The effective potential $\phi_{\rm eff}$ is plotted in Fig. 5(a) as a function of $\bar{a}_3$. For given $\bar{a}_1$, the minimum in $\phi_{\rm eff}$ determines an equilibrium value for $\bar{a}_3$. The relation between $\bar{a}_3$ and $\bar{a}_1$ in equilibrium is given by the axial force balance equation, Eq. (43b). We refer to the energy of this equilibrium as $\bar{\mathscr{H}}_\parallel^{\rm min}(\bar{a}_1)$, which is found by obtaining the solution of Eq. (43b) for $\bar{a}_3(\bar{a}_1)$ in equilibrium, and substituting this solution into $\phi_{\rm eff}(\bar{a}_3,\bar{a}_1)$.

An interesting artifact of our fluid model can be observed in $\phi_{\rm eff}$: it is finite even as $\bar{a}_3 \to 0$. This can be seen in Fig. 5(a), and the value of $\phi_{\rm eff}$ at $a_3 = 0$ can be determined from the limiting forms of A_1 and A_3:

$$\lim_{x\to 0} A_1(x) = \frac{\pi}{2}x, \quad \lim_{x\to 0} A_3(x) = 2 - \frac{\pi}{2}x,$$

and by substituting these limits into Eq. (45b) we obtain

$$\lim_{\bar{a}_3\to 0} \phi_{\rm eff} = \frac{\pi}{2\bar{a}_1}.$$

Thus, in our fluid model, the plasma can be made to collapse down to an infinitely thin disk during the motion if $\bar{\mathscr{H}}_\parallel \geqslant \pi/2\bar{a}_1$. An example of this behavior is presented in Fig. 3(b), which shows that the collapse can occur even if radial motion is kept in the dynamics. This actually has some physical significance: For sufficiently large energies, particles in the plasma have enough energy to transit through the x-y plane during the oscillations, "reversing" the plasma. If all the particles perform this maneuver precisely in phase, there is a point in time when the plasma is an infinitely thin disk. However, while such transiting of the x-y plane certainly would occur for some ions in a real plasma, extreme heating would be caused by such large compressions and expansions, with the result that the infinitely thin disk could never be achieved. Of course, the effect of plasma heating is neglected in the cold-fluid model used here. Thus, for large values of $\mathscr{H}_\parallel$, this model of the spheroidal dynamics must be regarded only as the simplest first approximation, and in particular the motion as $\bar{a}_3 \to 0$ is patently unphysical. We discuss one possible improvement of the model in Sec. II D.

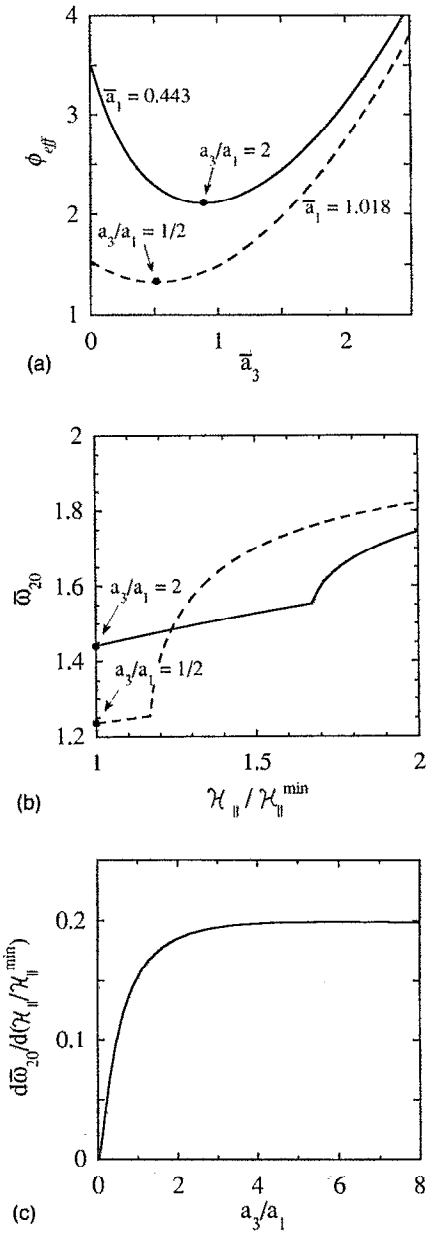

FIG. 5. Guiding-center limit of the finite-amplitude (2,0) modes. (a) The effective potential well, $\phi_{\rm eff}$, of the axial oscillations of a homogeneous spheroidal non-neutral plasma in the strong magnetic field (guiding-center) limit for two values of $\bar{a}_1$ [see Eq. (45b)]. Solid line: $\bar{a}_1 = 0.443$ corresponding to a prolate equilibrium shape given by $a_3/a_1 = 2$. Dashed line: $\bar{a}_1 = 1.018$, corresponding to the oblate equilibrium $a_3/a_1 = 1/2$. (b) Frequency of the axial oscillations, $\bar{\omega}_{20}$, versus amplitude for the two potentials shown in Fig. 3(a). Amplitude is measured as the ratio of the parallel energy to the potential energy evaluated at the potential minimum, $\mathscr{H}_\parallel / \mathscr{H}_\parallel^{\rm min}$. (c) The rate of change of $\bar{\omega}_{20}$ with respect to $\mathscr{H}_\parallel / \mathscr{H}_\parallel^{\rm min}$, evaluated in the small-amplitude limit $\mathscr{H}_\parallel / \mathscr{H}_\parallel^{\rm min} = 1$, as a function of equilibrium shape a_3/a_1.

As $\mathscr{H}_\parallel$ approaches $\mathscr{H}_\parallel^{\rm min}$, the turning points $\bar{a}_3^{(1)}$ and $\bar{a}_3^{(2)}$ approach one another and the oscillations of $\bar{a}_3$ reduce to the large $\bar{\Omega}_c$ limit of the linear (2,0) plasma oscillations described in Refs. 5–7. For arbitrary amplitude, the frequency ω_{20} of nonlinear plasma oscillations follows from Eq. (45):

$$\bar{\omega}_{20}(\bar{\mathscr{H}}_{\parallel},\bar{a}_1)$$

$$=\begin{cases}\pi \Big/ \displaystyle\int_{\bar{a}_3^{(1)}}^{\bar{a}_3^{(2)}} \frac{d\bar{a}_3}{\sqrt{2\bar{\mathscr{H}}_{\parallel}-2\phi_{\text{eff}}(\bar{a}_3,\bar{a}_1)}}, & \bar{\mathscr{H}}_{\parallel}<\pi/2\bar{a}_1, \\ \pi \Big/ \displaystyle\int_{0}^{\bar{a}_3^{(2)}} \frac{d\bar{a}_3}{\sqrt{2\bar{\mathscr{H}}_{\parallel}-2\phi_{\text{eff}}(\bar{a}_3,\bar{a}_1)}}, & \bar{\mathscr{H}}_{\parallel}>\pi/2\bar{a}_1. \end{cases} \tag{47}$$

Frequencies are plotted in Fig. 5(b) for two values of $\bar{a}_1$ as a function of the energy ratio $\mathscr{H}_{\parallel}/\mathscr{H}_{\parallel}^{\min}$. These two values of $\bar{a}_1$ are chosen to correspond to equilibrium shapes given by $a_3/a_1=1/2$ and $a_3/a_1=2$, through Eq. (43b). For small excitation amplitudes, $\bar{\omega}_{20}$ is approximately linear in $\mathscr{H}_{\parallel}/\mathscr{H}_{\parallel}^{\min}$, as one would expect for this anharmonic oscillator. The rate of change of $\bar{\omega}_{20}$ with $\mathscr{H}_{\parallel}/\mathscr{H}_{\parallel}^{\min}$ is displayed in Fig. 5(c) as a function of the equilibrium shape of the spheroid.

The kink in the behavior of $\bar{\omega}_{20}$ occurs at the point where the spheroid is flattened to a disk, i.e., where $\bar{a}_3^{(1)}$ vanishes. Finite pressure effects should be considered for amplitudes beyond this kink. We will now discuss one simple model for these effects.

D. Thermal effects

So far the effects of thermal pressure on the quadrupole motions have been neglected, which is a good approximation provided that the plasma's potential energy density $\mathscr{P}/V$ is much larger than the thermal pressure. However, we have seen that, for very large amplitudes, the nonlinear spheroidal oscillations display unphysical behavior connected to the omission of pressure forces—the cold-fluid plasma can collapse to an infinitely thin disk. The effects of thermal pressure on this motion can be added to our model in order to remove this unphysical behavior, provided that we are willing to make several further approximations. As is shown in Ref. 12, the ∇p term can be kept in Eq. (3a) without affecting the basic nature of our nine-degree-of-freedom system of equations, provided that the pressure is *assumed to be* a quadratic function of position within the plasma, taking the form in body axes

$$p(\mathbf{x}',t)=p_0(t)\left(1-\sum_{i=1}^{3}\frac{x_i^2}{a_i^2}\right),$$

where $p_0(t)$ is any function of time. One can easily show that this merely adds a term $2p_0(t)\mathbf{S}'^{-1}/mn$ to the right-hand side of Eq. (21).

This ansatz for $p(\mathbf{x},t)$ can be understood physically by considering an equivalent formulation of the quadrupole equations that follows from a virial expansion approach, in which moments of the Euler equations are taken.[12] The pressure $p_0(t)$ can be interpreted in this formulation as just 5/2 of the average pressure found by integrating p over the ellipsoid. This is a crude approximation since the actual pressure gradient is not linear in $\mathbf{x}'$ but is concentrated at the edge of the plasma where the density falls to zero. Nevertheless, the approximation retains some of the qualitative features of the effect of pressure on the plasma motions. In any case, if we then assume that some equation of state relates p_0 to the density, we can solve for the motions of the ellipsoid.

Unfortunately, such an equation of state is unknown in general, particularly for axial spheroidal oscillations which are at frequencies on the order of the plasma frequency. Such oscillations are in general neither adiabatic nor isothermal, although for a weakly correlated (collisionless) plasma the adiabatic approximation may be useful. Nevertheless, if we assume some simple adiabatic relation such as $p_0V^{\gamma}=\text{const}$ for some constant γ [where $V=(4/3)\pi a_1^2a_3$ is the plasma volume], the effect of p_0 on Eq. (41a) is to introduce a term $C'/[(\bar{a}_1^2\bar{a}_3)^{\gamma-1}\bar{a}_3]$ on the right-hand side, where C' is a constant related to the initial pressure and volume. For any $\gamma\geqslant 1$, this term clearly removes the possibility of collapse to $\bar{a}_3=0$. Incidentally, the Hamiltonian form of the equations is preserved, with a free energy term now appearing in the effective potential, of the form $C'/[(\gamma-1)(\bar{a}_1^2\bar{a}_3)^{\gamma-1}]$ for $\gamma>1$. For small initial temperature (i.e., $C'\ll 1$), this term slightly increases the frequency ω_{20} of the axial oscillations. In fact, Eq. (47) has the same form except that the free energy term modifies the effective potential so that the lower turning point $\bar{a}_3^{(1)}$ never reaches zero; this has the effect of smoothing out the kinks in Fig. 5(b).

This approach to finite temperature effects may be a useful first approximation, especially for weakly correlated (collisionless) plasmas, but it also has drawbacks—it neglects the effects of damping which could be significant for these very large amplitude oscillations, it neglects the effect of finite temperature on the equilibrium density profile, and it leaves open the question of what form to use for the high-frequency equation of state. The approach may be of more use in analyzing the effect of pressure on smaller-amplitude motions, or on the nonlinear equilibria discussed in the next section. We feel that the best way to test the effect of finite temperature is through molecular dynamics simulations of the quadrupole oscillations, particularly for the case of strongly correlated plasmas. Such simulations are currently underway and will be reported upon in a future paper.

III. EQUILIBRIUM CONFIGURATIONS

In this section, we consider the equilibrium configurations of a homogeneous ellipsoidal non-neutral plasma confined in a cylindrically symmetric Penning trap. By equilibrium we mean a state in which the plasma's shape and density are time independent in some frame rotating with constant rotation frequency $\boldsymbol{\omega}$. Furthermore, in this frame there may remain an internal fluid flow described by a time-independent internal rotation Λ; however, this flow leaves the shape of the ellipsoid unchanged.

In Sec. III A, we obtain the equations describing such ellipsoidal equilibria and derive a non-neutral plasma version of Riemann's theorem, with which we classify the equilibria into two types, which we refer to as aligned and tilted ellipsoids. The aligned ellipsoids have a body axis parallel to $\hat{\mathbf{z}}$ and also have $\boldsymbol{\omega}\|\hat{\mathbf{z}}\|\Lambda$. As we discussed in the Introduction, these ellipsoids can be thought of as finite-amplitude extensions of the (2,2) quadrupole normal

modes,[5-7] a typical solution is depicted schematically in Fig. 2(c). The tilted ellipsoids are also characterized by $\boldsymbol{\omega} \| \hat{\mathbf{z}}$, but now $\boldsymbol{\Lambda}$ is not parallel to $\hat{\mathbf{z}}$. Rather, $\boldsymbol{\omega}$ and $\boldsymbol{\Lambda}$ lie in a principal plane of the ellipsoid. These solutions correspond to ellipsoids that are tilted with respect to the laboratory z axis by an angle θ, and which precess around the axis with rotation frequency ω. They can be thought of as finite-amplitude extensions of the (2,1) quadrupole normal modes [see Fig. 2(b)].

We find that both the aligned and tilted ellipsoids can be parametrized by the shape of the ellipsoid as described by the variables $(a_2/a_1, a_3/a_1)$, and $\bar{\Omega}_c = \Omega_c/\omega_z$. In other words, when these three variables are specified we obtain a finite set of aligned and tilted solutions, with all other parameters such as ω, ω_p, Λ, and θ determined in terms of these variables.

In Secs. III B and III C, we present an analysis of the behavior of these aligned and tilted ellipsoids, paying particular attention to the regimes of existence of solutions. The boundaries of these regions are generalizations of the well-known Brillouin limit for rigid-rotor axisymmetric equilibria, given by $\omega_p^2 \leqslant \Omega_c^2/2$. In fact, the discovery of non-axisymmetric equilibria with internal fluid shears allows considerably more latitude in the possible densities that can be confined in equilibrium for given external applied fields.

A. Equilibrium equations and Riemann's theorem for a non-neutral plasma

The condition that the ellipsoid be in equilibrium demands that the rotation frequency $\boldsymbol{\omega}$ must be parallel to $\hat{\mathbf{z}}$. This follows from the cylindrical symmetry of the external fields, which implies that, in the frame rotating with the body axes, the field tensors $\boldsymbol{\epsilon}_e'$ and $\boldsymbol{\Omega}_c^*$ are independent of ϕ but do depend on θ and ψ. In equilibrium, $\dot{\theta}$ and $\dot{\psi}$ must therefore vanish, otherwise the external fields become time dependent in the body axis frame. However, $\dot{\phi}$ need not vanish, so $\boldsymbol{\omega}$ and $\hat{\mathbf{z}}$ must be parallel. On the other hand, we will soon see that neither $\boldsymbol{\zeta}$ nor $\boldsymbol{\Lambda}$ need be parallel to $\hat{\mathbf{z}}$ in equilibrium, so nontrivial internal fluid motions can occur.

However, before we consider the general equilibrium equations, we first obtain a simple relation between the density of the rotating equilibrium and the velocity of the fluid. Dropping the time derivatives in Eq. (21), we take the trace after acting on the right with $\mathbf{S}'^{-1}$. Since $\mathrm{Tr}(\boldsymbol{\epsilon}_p') = 1$ and $\mathrm{Tr}(\boldsymbol{\epsilon}_e') = 0$, we find

$$\omega_p^2 = \mathrm{Tr}[\mathbf{S}' \cdot \boldsymbol{\Lambda}^{*2} \cdot \mathbf{S}'^{-1} + \boldsymbol{\omega}^{*2} - (\boldsymbol{\Omega}_c^* + 2\boldsymbol{\omega}^*) \cdot \mathbf{S}' \cdot \boldsymbol{\Lambda}^* \cdot \mathbf{S}'^{-1} + \boldsymbol{\Omega}_c^* \cdot \boldsymbol{\omega}^*].$$

However, $\mathrm{Tr}(\mathbf{S}' \cdot \boldsymbol{\Lambda}^{*2} \cdot \mathbf{S}'^{-1}) = \mathrm{Tr}\,\boldsymbol{\Lambda}^{*2} = -2\Sigma_i \Lambda_i^2$, where Eq. (19) is used in the last step. Similarly, $\mathrm{Tr}\,\boldsymbol{\omega}^{*2} = -2\Sigma_i \omega_i^2$ and $\mathrm{Tr}(\boldsymbol{\Omega}_c^* \cdot \boldsymbol{\omega}^*) = -2\Sigma_i \Omega_c z_i \omega_i$. Furthermore, the third term can be simply expressed in terms of the internal vorticity using Eqs. (8b), (13), (19), and (20):

$$\mathrm{Tr}[(\boldsymbol{\Omega}_c^* + 2\boldsymbol{\omega}^*) \cdot \mathbf{S}' \cdot \boldsymbol{\Lambda}^* \cdot \mathbf{S}'^{-1}] = \sum_i \zeta_i \Omega_{v_i}.$$

Combining these results, we find a general expression for the plasma frequency of the equilibrium ellipsoid:

$$\omega_p^2 = -2\omega(\Omega_c + \omega) - 2\Lambda^2 - \Omega_v \hat{\mathbf{z}} \cdot \boldsymbol{\zeta}, \tag{48}$$

where we have also used the fact that $\boldsymbol{\omega} \| \hat{\mathbf{z}}$. The first term is the usual result for the plasma frequency in a rigid-rotor equilibrium, and the second and third terms are corrections due to internal motions in the ellipsoid. As we discussed in relation to Eq. (44), for cylindrically symmetric rigid-rotor equilibria the rotation frequency of the body axes is undefined, and in this case it is common practice to choose ω so that the plasma is at rest in the rotating frame ($\Lambda = \zeta = 0$). Any other rotating frame could also be chosen in which case Λ and ζ would be nonzero and Eq. (48) shows that ω_p^2 is invariant under such choices.

The maximum possible value of the first term occurs at the Brillouin limit, $\omega = -\Omega_c/2$, which implies $\max(\omega_p^2) = \Omega_c^2/2$ for rigid-rotor equilibria. However, the addition of internal motions changes this result, and we will see that non-rigid-rotor equilibria exist for which ω_p^2 exceeds the Brillouin limit.

The general equations for ellipsoidal equilibrium are found by taking $\boldsymbol{\omega} \| \hat{\mathbf{z}}$ and dropping time derivatives in Eqs. (24):

$$-\sum_{k \neq i} \bar{\Lambda}_k^2 + \beta - \frac{\bar{\omega}_p^2}{2} A_i + (1-\beta) z_i^2 + \frac{\bar{\Omega}_v}{a_i} \sum_{j \neq k \neq i} a_j \bar{\Lambda}_k z_k = 0 \tag{49a}$$

and

$$\frac{a_i}{a_j} \bar{\Lambda}_i \bar{\Lambda}_j + (1-\beta) z_i z_j - \bar{\Omega}_v \bar{\Lambda}_i z_j \frac{a_k}{a_j} = 0 \quad (i \neq j \neq k). \tag{49b}$$

Here, we have introduced the trap parameter β defined by

$$\beta \equiv -\bar{\omega}(\bar{\Omega}_c + \bar{\omega}) - \tfrac{1}{2} = \tfrac{1}{4}(\bar{\Omega}_c^2 - \bar{\Omega}_v^2) - \tfrac{1}{2}, \tag{50}$$

and we have employed the relation $\hat{z}^2 = z_1^2 + z_2^2 + z_3^2 = 1$. For a rigid-rotor equilibrium, β is the ratio of the total confining force in the radial direction to that in the z direction, so β determines the shape, a_3/a_1, of a rigid-rotor plasma [see Eq. (44)].

We will now consider several linear combinations of the off-diagonal elements, Eq. (49b), from which some general requirements for the equilibrium configuration follow. Adding and subtracting the $(i,j) = (2,3)$ term multiplied by a_3^2 and the (3,2) term multiplied by a_2^2 yields the equations

$$z_2 z_3 (a_3^2 + a_2^2)(1-\beta) - \bar{\Omega}_v a_1 (\bar{\Lambda}_2 a_3 z_3 + \bar{\Lambda}_3 a_2 z_2) + 2 a_2 a_3 \bar{\Lambda}_2 \bar{\Lambda}_3 = 0 \tag{51}$$

and

$$z_2 z_3 (a_3^2 - a_2^2)(1-\beta) - \bar{\Omega}_v a_1 (\bar{\Lambda}_2 a_3 z_3 - \bar{\Lambda}_3 a_2 z_2) = 0. \tag{52}$$

Let us consider the most general possible configuration, in which all three components of $\bar{\boldsymbol{\Lambda}}$ and all the components of $\hat{\mathbf{z}}$ (as seen in the body frame) are nonzero, so that the ellipsoid is oriented in any manner and the internal vorticity vector is also oriented in some arbitrary direction. We

will show that this general configuration is, in fact, impossible to achieve in equilibrium, and we will derive restrictions on the orientation of the body axes and $\bar{\Lambda}$. As we have assumed that z_2 and z_3 are nonzero, we divide through by z_2 and z_3 in Eqs. (51) and (52) and define new variables $\alpha_i \equiv \bar{\Lambda}_i/\bar{\Omega}_v z_i$. The resulting equations for α_2 and α_3 are independent of the Euler angles and may be reduced to two quadratics:

$$\bar{\Omega}_v^2\alpha_2^2+\frac{\alpha_2}{a_1a_3}[(a_2^2-a_3^2)(1-\beta)-a_1^2\bar{\Omega}_v^2]+1-\beta=0, \tag{53}$$

$$\bar{\Omega}_v^2\alpha_3^2+\frac{\alpha_3}{a_1a_2}[-(a_2^2-a_3^2)(1-\beta)-a_1^2\bar{\Omega}_v^2]+1-\beta=0. \tag{54}$$

However, if we now consider the sum and difference of the (1,2) component of Eq. (49b) multiplied by a_2^2 and the (2,1) equation multiplied by a_1^2, we find two similar relations for α_2 and α_1, assuming here that z_1 and z_2 are nonzero:

$$\begin{aligned}\bar{\Omega}_v^2\alpha_1^2+\frac{\alpha_1}{a_2a_3}[(a_1^2-a_2^2)(1-\beta)-a_3^2\bar{\Omega}_v^2]+1-\beta=0,\\ \bar{\Omega}_v^2\alpha_2^2+\frac{\alpha_2}{a_1a_3}[-(a_1^2-a_2^2)(1-\beta)-a_3^2\bar{\Omega}_v^2]+1-\beta=0.\end{aligned} \tag{55}$$

Subtracting Eq. (53) from Eq. (55) yields

$$\frac{\alpha_2(a_3^2-a_1^2)}{a_1a_3}(1-\beta-\bar{\Omega}_v^2)=0.$$

Furthermore, consideration of the (1,3) and (3,1) equations leads to the analogous results

$$\frac{\alpha_1(a_2^2-a_3^2)}{a_2a_3}(1-\beta-\bar{\Omega}_v^2)=0,$$

$$\frac{\alpha_3(a_1^2-a_2^2)}{a_1a_2}(1-\beta-\bar{\Omega}_v^2)=0.$$

Thus, if we assume all three components of $\hat{\mathbf{z}}$ are nonzero in the body frame, we are led to the conclusion that either $a_1=a_2=a_3$ (a degenerate case since any orientation of the body axes is allowed), $1-\beta=\bar{\Omega}_v^2$, or $\bar{\Lambda}=0$. The case $\bar{\Lambda}=0$ is also trivial since Eqs. (49) imply that, in this case, the plasma must be a rigid-rotor spheroid. The case $1-\beta=\bar{\Omega}_v^2$ is more complicated, but we will show in Sec. III C that this case is also degenerate, corresponding to a spheroidal equilibrium that allows for an arbitrary rotation of the body axes about the axis of symmetry of the spheroid.

For a nontrivial solution, we therefore require that at least one of the pairs $(z_1,\bar{\Lambda}_1)$, $(z_2,\bar{\Lambda}_2)$, $(z_3,\bar{\Lambda}_3)$ must be equal to zero. This result is known as Riemann's theorem when applied to force-free gravitational equilibria.[12] Here, we see that the theorem also holds for ellipsoidal plasmas confined by the cylindrically symmetric external fields of a Penning trap. An alternative statement of the theorem is that equilibrium demands that either Λ and $\hat{\mathbf{z}}$ are parallel, in which case they lie along a principal axis of the ellipsoid, or they are not parallel, in which case they lie in a principal plane of the ellipsoid. We refer to the former class of equilibria as aligned ellipsoids and the latter class as the tilted ellipsoids. We will see that the aligned ellipsoids *cannot* be obtained as a special case of the tilted ellipsoids in the limit that the angle between Λ and $\hat{\mathbf{z}}$ vanishes. Note that, although Λ and ζ are not necessarily parallel, one can substitute ζ for Λ in the statement of the theorem.

B. Aligned ellipsoids

We first consider the aligned ellipsoids in which $\hat{\mathbf{z}}$, ω and Λ are parallel and are oriented along a principal axis, which we take to be the $\hat{\mathbf{e}}_3$ axis without loss of generality. Thus only the $\hat{\mathbf{e}}_3$ components of ω and Λ are nonzero, and the $\hat{\mathbf{e}}_3$ axis is parallel to $\hat{\mathbf{z}}$. In this case, Eq. (49b) is satisfied trivially. The diagonal elements, Eq. (49a), are

$$-\bar{\Lambda}_3^2+\beta-\frac{\bar{\omega}_p^2}{2}A_1+\bar{\Omega}_v\frac{a_2}{a_1}\bar{\Lambda}_3=0, \tag{56a}$$

$$-\bar{\Lambda}_3^2+\beta-\frac{\bar{\omega}_p^2}{2}A_2+\bar{\Omega}_v\frac{a_1}{a_2}\bar{\Lambda}_3=0, \tag{56b}$$

$$1-\frac{\bar{\omega}_p^2}{2}A_3=0. \tag{56c}$$

Equations (56) are expressions of equilibrium force balance in the $\hat{\mathbf{e}}_1$, $\hat{\mathbf{e}}_2$, and $\hat{\mathbf{e}}_3$ body axis directions, and so may be regarded as generalizations of the expressions for axial and radial force balance, Eqs. (43), derived for a rigid-rotor spheroid. We could also have obtained these equations by setting time derivatives equal to zero in Eqs. (39). Indeed, when $a_1=a_2$ then $A_1=A_2$ and Eqs. (56a) and (56b) are identical, and can be shown to be equivalent to Eq. (43a) with the aid of Eqs. (27), (31), and (38).

Thus, when $a_1=a_2$, the aligned equilibria reduce to rigid-rotor spheroids whose shape, a_3/a_1, is determined by Eq. (44). Since the internal motion set up by $\bar{\Lambda}$ is merely an extra rigid rotation in this case, we absorb $\bar{\Lambda}$ into the definition of $\bar{\omega}$, so that Eq. (44) becomes[1]

$$-\bar{\omega}(\bar{\Omega}_c+\bar{\omega})-\frac{1}{2}=\frac{A_1}{A_3},$$

or $\beta=A_1/A_3$. This is a quadratic equation for $\bar{\omega}$ with two solutions most economically expressed in terms of the vortex frequency $\bar{\Omega}_v=\bar{\Omega}_c+2\bar{\omega}$:

$$\bar{\Omega}_v^2=\bar{\Omega}_c^2-4A_1/A_3-2=\bar{\Omega}_c^2-4/A_3, \tag{57}$$

where in the last step we used the relation $2A_1+A_3=2$ [see Eq. (A4)].

Equation (57) implies that a minimum magnetic field strength is required to confine a spheroid of given shape:

$$\bar{\Omega}_c^2>4/A_3(a_3/a_1). \tag{58}$$

We plot the minimum value of $\bar{\Omega}_c^2$ vs a_3/a_1 in Fig. 6. This figure shows the region of existence of rigid-rotor spheroidal equilibria in the parameter space $(a_3/a_1,\bar{\Omega}_c)$. The figure also shows that the rigid-rotor case is a special case of the

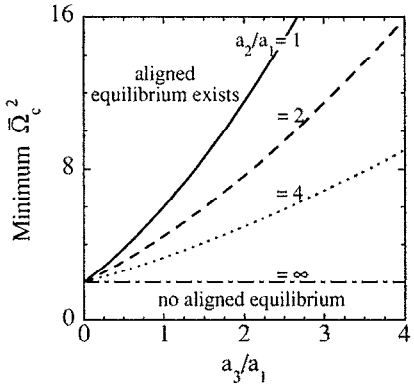

FIG. 6. Minimum possible value of $\bar{\Omega}_c^2$ required to confine an aligned ellipsoid versus a_3/a_1 for four values of a_2/a_1. The rigid-rotor spheroid case corresponding to the Brillouin limit, Eq. (58), is the $a_2/a_1=1$ curve (solid curve). This curve also describes the behavior of M (see Fig. 13 and Sec. III C).

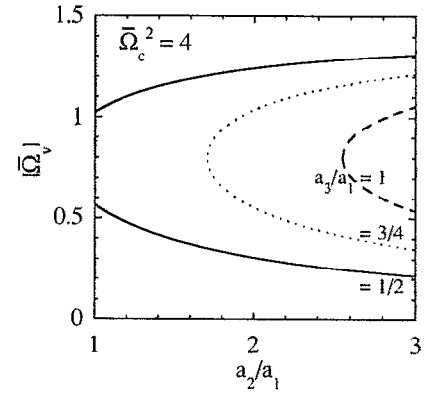

FIG. 7. Behavior of the two solutions of Eq. (60) for the vortex frequency of the aligned ellipsoids as a function of degree of ellipsoidal distortion, as measured by a_2/a_1, for three values of a_3/a_1 and for $\bar{\Omega}_c=2$. As a_2/a_1 approaches unity, the ellipsoid approaches a rigid-rotor spheroid with a (2,2) normal mode perturbation added. Solid line: $a_3/a_1=0.5$ (density below the Brillouin limit: see Fig. 6). Dotted line: $a_3/a_1=0.75$. Dashed line: $a_3/a_1=1$. In the latter two cases, a rigid-rotor spheroidal equilibrium no longer exists (see Fig. 6).

more general existence region for aligned ellipsoids with $a_2/a_1\neq 1$, which we will discuss presently.

Now, from Eq. (56c) the plasma frequency can be expressed in terms of the shape as $\bar{\omega}_p^2=2/A_3$. When this is compared to Eq. (58), we find $\Omega_c^2\geq 2\omega_p^2$, which is just the Brillouin limit for the maximum density achievable in a given magnetic field. We also observe that the maximum possible value of A_3 is 2 [see Eq. (A4)], so Eq. (58) implies no rigid-rotor equilibrium exists if $\bar{\Omega}_c^2<2$. In this regime, the confining force of the magnetic field cannot overcome the repulsive radial trap field and the centrifugal force due to rotation, even if only a single particle is confined in the trap. The addition of more particles that repel one another can only further reduce the confinement, so the condition $\bar{\Omega}_c^2>2$ applies to all equilibria.

Turning now to the case $a_1\neq a_2$, Eqs. (56) describe a triaxial ellipsoid rotating about the z axis, together with an internal vorticity in the $\hat{\mathbf{z}}$ direction, causing a shear in the internal fluid velocity of the ellipsoid. This motion is a finite-amplitude generalization of the (2,2) linear diocotron and cyclotron modes discussed in Refs. 6 and 7. Proceeding with the analysis of the properties of this rotating equilibrium, we divide Eqs. (56a) and (56b) by $\bar{\Omega}_v^2$, substitute for ω_p^2 using Eq. (56c), and add and subtract the resulting equations to find that $\bar{\Lambda}_3/\bar{\Omega}_v$ must satisfy the relations

$$\left(\frac{\bar{\Lambda}_3}{\bar{\Omega}_v}\right)^2-\frac{\beta}{\bar{\Omega}_v^2}+\frac{A_1+A_2}{2A_3\bar{\Omega}_v^2}-\frac{1}{2}\frac{\bar{\Lambda}_3}{\bar{\Omega}_v}\frac{a_1^2+a_2^2}{2a_1a_2}=0 \tag{59a}$$

and

$$\frac{A_1-A_2}{\bar{\Omega}_v^2A_3}+\frac{\bar{\Lambda}_3}{\bar{\Omega}_v}\frac{a_1^2-a_2^2}{a_1a_2}=0. \tag{59b}$$

Equation (59b) determines $\bar{\Lambda}_3/\bar{\Omega}_v$ in terms of $\bar{\Omega}_v^2$ and the shape variables $(a_2/a_1,a_3/a_1)$. Substituting this result into (59a) leads to a quadratic equation for $\bar{\Omega}_v^2$ in terms of a_2/a_1 and a_3/a_1:

$$\bar{\Omega}_v^4-D\bar{\Omega}_v^2+E=0, \tag{60a}$$

where the coefficients D and E are defined as

$$D\equiv\frac{-4}{A_3}+\frac{2(A_1-A_2)(a_1^2+a_2^2)}{A_3(a_2^2-a_1^2)}+\bar{\Omega}_c^2, \tag{60b}$$

and

$$E\equiv\frac{4(A_1-A_2)^2}{A_3^2}\frac{a_1^2a_2^2}{(a_2^2-a_1^2)^2}. \tag{60c}$$

The two solutions of Eq. (60) for $|\bar{\Omega}_v|$ are plotted in Fig. 7 as a function of a_2/a_1 for $\bar{\Omega}_c=2$.

We plot $|\bar{\Omega}_v|$ rather than the rotation frequency ω of the equilibrium since $|\bar{\Omega}_v|$ is the more natural variable in the following sense. The rotation frequency of the body axes is related to the plotted curves in Fig. 7 through $\omega=(\pm|\Omega_v|-\Omega_c)/2$, so for given a_2/a_1, a_3/a_1, and $\bar{\Omega}_c$ there are *four* possible rotation frequencies. These four frequencies correspond to excitation of the two linear (2,2) modes around either of the two rigid-rotor equilibria that have shape a_3/a_1. In other words, by plotting $|\Omega_v|$ rather than ω we make use of the symmetry of the solutions discussed in relation to Eq. (22) under the transformation $\Omega_v\rightarrow-\Omega_v$, $\Lambda\rightarrow-\Lambda$, and the four solutions for ω are reduced to two solutions for $|\Omega_v|$.

For large $\bar{\Omega}_c$, one root of Eq. (60) for $|\bar{\Omega}_v|$ is of order $|\bar{\Omega}_c|$ and the other is of order $|1/\bar{\Omega}_c|$. For $\bar{\Omega}_v>0$, the former root is a low rotation frequency $\mathbf{E}\times\mathbf{B}$ drift solution corresponding to a finite-amplitude generalization of the (2,2) diocotron mode. The rotation frequency of this nonlinear diocotron mode is, to order $1/\bar{\Omega}_c$, given by $\bar{\Omega}_v^2=D$, which implies

$$\frac{\omega\Omega_c}{\omega_z^2}=\frac{-1}{A_3}+\frac{A_1-A_2}{2A_3}\frac{(a_1^2+a_2^2)}{a_2^2-a_1^2}+O\left(\frac{1}{\bar{\Omega}_c}\right). \tag{61}$$

The diocotron mode is usually considered on an infinite-length column rather than an ellipsoid, and so it is

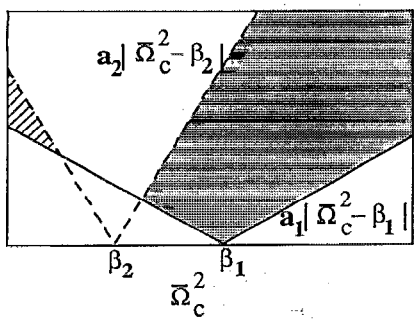

FIG. 8. Gray and cross-hatched regions are the areas where $a_2|\bar{\Omega}_c^2-\beta_2|\geq a_1|\bar{\Omega}_c^2-\beta_1|$ for the case where $a_2>a_1$ [see discussion preceding Eq. (63)]. The cross-hatched region is disallowed by the constraint $D\geq 0$.

useful to obtain the infinite-length limit of the nonlinear diocotron mode rotation frequency. In this limit, $a_3/a_1\to\infty$ as $\omega_z\to 0$, so in Eq. (61) we substitute for ω_z^2 in terms of ω_p^2 through Eq. (56c). If we also substitute in the form for A_1 and A_2 in the limit that $a_3/a_1\to\infty$ [see Eqs. (A8)], we find that

$$\omega=-\frac{\omega_p^2}{\Omega_c}\frac{a_1a_2}{(a_1+a_2)^2}. \tag{62}$$

This result can be identified as the rotation frequency of an elliptical patch of vorticity in an inviscid fluid flow described by the 2-D Euler equations (the Kirchhoff vortex). This follows from a well-known isomorphism between the 2-D Euler equations and 2-D $\mathbf{E}\times\mathbf{B}$ drift equations.[19,20] When $a_1\to a_2$, the usual infinite-length $m=2$ linear diocotron mode result is recovered: $\omega\Omega_c=-\omega_p^2/4$.[21]

In order to confine an aligned ellipsoid of a given shape, a magnetic field exceeding a certain minimum field strength must be applied. A relation can be found for the minimum $\bar{\Omega}_c^2$ value as a function of the ellipsoid shape variables $(a_2/a_1,a_3/a_1)$. Equations (60) imply that, in order that a real solution for $\bar{\Omega}_v$ exist, D must be non-negative and D^2-4E must also be non-negative. Both inequalities place requirements on the minimum possible allowed cyclotron frequency for a given ellipsoid shape. However, the second inequality places a more stringent requirement on $\bar{\Omega}_c^2$. After some algebra, one can show that $D^2-4E\geq 0$ can be written as

$$\frac{a_2^2[\bar{\Omega}_c^2A_3+2(A_1-A_2)-4]^2-a_1^2[\bar{\Omega}_c^2A_3-2(A_1-A_2)-4]^2}{A_3^2(a_2^2-a_1^2)}$$

$$\geq 0.$$

This expression is clearly symmetric upon interchange of (a_1,A_1) and (a_2,A_2) so without loss of generality we assume that $a_2>a_1$. In this case, there follows the relation

$$a_2|\bar{\Omega}_c^2-\beta_2|\geq a_1|\bar{\Omega}_c^2-\beta_1|,$$

where $\beta_{1\atop(2)}\equiv[4\pm 2(A_1-A_2)]/A_3$. The region of $\bar{\Omega}_c^2$ for which the inequality is satisfied is shown in Fig. 8. Since $a_2>a_1$ was assumed, $A_2<A_1$ and $\beta_1>\beta_2$ so it is apparent from Fig. 8 that the inequality is satisfied for values of $\bar{\Omega}_c^2$ determined by $a_2(\bar{\Omega}_c^2-\beta_2)\geq -a_1(\bar{\Omega}_c^2-\beta_1)$, or $\bar{\Omega}_c^2\geq(a_1\beta_1+a_2\beta_2)/(a_1+a_2)$. These values of $\bar{\Omega}_c^2$ correspond to the gray region of Fig. 8. The cross-hatched area is disallowed by the inequality $D\geq 0$. The cyclotron frequency must therefore be sufficiently large so that

$$\bar{\Omega}_c^2\geq\frac{4}{A_3}-\frac{2(A_1-A_2)}{A_3}\frac{a_2-a_1}{a_2+a_1} \tag{63}$$

in order for either of the aligned equilibria to exist. The lower bound of Eq. (63) gives the minimum cyclotron frequency required to confine an ellipsoid of given shape and is plotted in Fig. 6. The result returns to the rigid-rotor spheroidal limit, Eq. (58), as $a_2/a_1\to 1$.

From Fig. 6, one can see that, for given a_3/a_1, the minimum possible value of $\bar{\Omega}_c^2$ occurs as $a_2/a_1\to\infty$. This minimum value can be found with the aid of Eq. (A4), and the fact that A_2 vanishes as $a_2/a_1\to\infty$. Equation (63) then becomes $\bar{\Omega}_c^2\geq 2$. For $\bar{\Omega}_c^2$ below this value, no equilibrium exists, just as in the case of the rigid-rotor spheroids.

Equation (63) leads to a simple result for the maximum density of an aligned ellipsoid for given external fields. For given shape, the plasma frequency may be obtained from Eq. (56c): $\bar{\omega}_p^2=2/A_3$. Dividing this equation by Eq. (63) we have

$$\omega_p^2\leq\Omega_c^2\Big/\left(2-(A_1-A_2)\frac{(a_2-a_1)}{a_1+a_2}\right). \tag{64}$$

Therefore, for a given magnetic field, the maximum possible density achievable is the same in either of the equilibria described by Eq. (60), and this density is larger than the Brillouin limit for a rigidly rotating spheroidal plasma. For given a_3/a_1, the maximum density occurs in the limits $a_1\gg a_2$ or $a_2\gg a_1$. As $a_2/a_1\to\infty$, $\bar{\Omega}_c^2\to 2$, which implies the maximum plasma frequency is $\omega_{p_{\max}}^2=\Omega_c^2/A_3$. If, in addition, the plasma is very prolate with $a_3\gg a_1$, then $A_3\to 0$ and ω_p^2/Ω_c^2 can approach infinity in equilibrium. This result is sensible (in the context of ideal fluid theory) because in this case the plasma approaches a 2-D slab that lies parallel to the magnetic field, and there is no Brillouin limit on the density in such a non-neutral plasma slab equilibrium. This is because the Brillouin limit stems from a competition between the deconfining centrifugal force due to rotation, and the confining $\mathbf{v}\times\mathbf{B}$ force.[10] However, in slab geometry there is no rotation, only a sheared velocity flow that can provide confinement for all densities, provided that the velocities are sufficiently large.

We have found that high-density nonaxisymmetric rotating ellipsoids are equilibrium solutions, but we have not considered the stability of such equilibria. Indeed, for a_2 different than a_1, the plasma no longer rotates rigidly and viscosity drives the system back to a rigid-rotor equilibrium. On a much shorter time scale, fluid instabilities can set in if the fluid velocity shear is sufficiently large. Such ideal fluid instabilities will be considered in a following paper. Some results are already known. For example, for the case of the slow rotation mode with $\bar{\Omega}_c\gg 1$ and with infinite length described by Eq. (62), the equilibrium has been shown to be stable for $a_2/a_1<3$.[19,22] The finite thresh-

old for onset of such ideal instabilities should allow the attainment of relatively long-lived states with densities larger than the Brillouin limit.

C. Tilted ellipsoids

We now consider the second type of ellipsoidal fluid equilibrium covered by the non-neutral plasma version of Riemann's theorem, in which $\mathbf{\Lambda}$ and $\hat{\mathbf{z}}$ are not parallel, but lie in a principal plane of the ellipsoid. That is, the ellipsoid is tilted with respect to the magnetic field direction $\hat{\mathbf{z}}$, and there is a component of the fluid velocity $\mathbf{v}$ in the $\hat{\mathbf{z}}$ direction [see Fig. 2(b)]. This equilibrium can be considered to be a finite-amplitude extension of a (2,1) linear normal mode. We will explore the regions of existence of the tilted ellipsoids in the parameter space defined by the three variables $\bar{\Omega}_c$, a_2/a_1, and a_3/a_1. For given values of these parameters, we will find at most three equilibrium solutions. We will derive simple limiting forms for these equilibria as $\bar{\Omega}_c \to \infty$. Furthermore, for special values of a_3/a_1, a_2/a_1, and $\bar{\Omega}_c$, we will encounter tilted ellipsoids that are stationary in the laboratory frame (that is, $\omega=0$) with a nonzero internal vorticity ζ; i.e., the Dedekind ellipsoids. As in the case of $\Lambda \| \hat{\mathbf{z}}$, we will find that tilted triaxial equilibria exist that exceed the Brillouin density limit for rigidly rotating spheroids. Finally, we will discover a set of tilted prolate spheroidal equilibria that occur only for $3 \leqslant \bar{\Omega}_c^2 \leqslant 6$.

Without loss of generality, we choose $(z_1,\Lambda_1)=0$ so that the internal vorticity vector lies in the $(\hat{\mathbf{e}}_1,\hat{\mathbf{e}}_2)$ plane and the Euler angle ψ vanishes. Thus, in what follows, $z_2=\sin\theta$ and $z_3=\cos\theta$, where θ is the angle of tilt of the three-body axis with respect to the magnetic field. The equilibrium equations are then given by Eqs. (53), (54), and (49a). Equations (49a) are written out explicitly below in terms of the previously defined parameter $\alpha_i=\bar{\Lambda}_i/\bar{\Omega}_v z_i$:

$$-\bar{\Omega}_v^2(\alpha_2^2\sin^2\theta+\alpha_3^2\cos^2\theta)+\beta-\frac{\bar{\omega}_p^2}{2}A_1 + \frac{\bar{\Omega}_v^2}{a_1}(a_2\alpha_3\cos^2\theta+a_3\alpha_2\sin^2\theta)=0, \tag{65a}$$

$$-\bar{\Omega}_v^2\alpha_3^2\cos^2\theta+\beta-\frac{\bar{\omega}_p^2}{2}A_2+(1-\beta)\sin^2\theta + \frac{\bar{\Omega}_v^2}{a_2}a_1\alpha_3\cos^2\theta=0, \tag{65b}$$

$$-\bar{\Omega}_v^2\alpha_2^2\sin^2\theta+\beta-\frac{\bar{\omega}_p^2}{2}A_3+(1-\beta)\cos^2\theta + \frac{\bar{\Omega}_v^2}{a_3}a_1\alpha_2\sin^2\theta=0. \tag{65c}$$

We begin the reduction of these coupled equations by solving for the plasma frequency using Eq. (65c):

$$\bar{\omega}_p^2=\frac{2}{A_3}\left[1+\sin^2\theta\left(-\bar{\Omega}_v^2\alpha_2^2-(1-\beta)+\bar{\Omega}_v^2\frac{a_1}{a_3}\alpha_2\right)\right].$$

This equation can be simplified by substituting for α_2^2 via Eq. (53):

$$\bar{\omega}_p^2=\frac{2}{A_3}\left(1-\frac{\alpha_2}{a_3/a_1}\bar{\Omega}_v^2 u\sin^2\theta\right), \tag{66}$$

where we introduce the parameter

$$u\equiv(a_3^2-a_2^2)(1-\beta)/(a_1^2\bar{\Omega}_v^2) \tag{67}$$

in order to simplify some of the subsequent algebra in the analysis of the equilibria. Now we substitute Eq. (66) into Eq. (65b) and into the difference between Eq. (65a) and (65b) [which is simpler than (65a) alone]. The results may be written as two linear equations in $\sin^2\theta$, which must be satisfied in order to achieve a tilted equilibrium. The equilibrium equations are

$$\delta_1\sin^2\theta+\delta_2=0, \tag{68a}$$

$$\gamma_1\sin^2\theta+\gamma_2=0, \tag{68b}$$

where the coefficients γ_i and δ_i are functions of a_2/a_1, a_3/a_1, $\bar{\Omega}_c^2$, and $\bar{\Omega}_v^2$:

$$\delta_1=u\bar{\Omega}_v^2\left(\frac{\alpha_2}{a_3/a_1}\frac{A_2}{A_3}-\frac{\alpha_3}{a_2/a_1}\right), \tag{68c}$$

$$\delta_2=1-\frac{A_2}{A_3}+u\bar{\Omega}_v^2\frac{\alpha_3}{a_2/a_1}, \tag{68d}$$

$$\gamma_1=\bar{\Omega}_v^2\left[-\frac{u\alpha_2}{a_3/a_1}\frac{A_2+A_3-A_1}{A_3} + \left[\left(\frac{a_3}{a_1}-\frac{a_1}{a_3}\right)\alpha_2-\left(\frac{a_2}{a_1}-\frac{a_1}{a_2}\right)\alpha_3\right]\right], \tag{68e}$$

$$\gamma_2=\frac{A_2-A_1}{A_3}+\bar{\Omega}_v^2\left(\frac{a_2}{a_1}-\frac{a_1}{a_2}\right)\alpha_3. \tag{68f}$$

These coefficients have been simplified by substituting for α_2^2 and α_3^2 using Eqs. (53) and (54), in a manner similar to the derivation of Eq. (66). We have also substituted for β in terms of the parameter u.

Equations (68a) and (68b) must be satisfied simultaneously, which requires that

$$\gamma_1\delta_2-\gamma_2\delta_1=0. \tag{69}$$

This is the general equation for tilted equilibria. In order to solve this equation, we also require the solutions of Eqs. (53) and (54) for α_2 and α_3, which are particularly simple when written in terms of u:

$$\alpha_2=(1+u\pm\lambda)/(2a_3/a_1), \tag{70a}$$

$$\alpha_3=(1-u\pm\lambda)/(2a_2/a_1), \tag{70b}$$

where

$$\lambda^2=\left(u-\frac{a_3+a_2}{a_3-a_2}\right)\left(u-\frac{a_3-a_2}{a_3+a_2}\right) \tag{70c}$$

and where the $\pm$ signs go together. Equation (69) must then be solved for $\bar{\Omega}_v^2$ in terms of the parameters a_2/a_1, a_3/a_1, and $\bar{\Omega}_c^2$ (note that u is a function of $\bar{\Omega}_c^2$, $\bar{\Omega}_v^2$, a_2/a_1, and a_3/a_1). The solution has several additional conditions

attached. First, $\bar{\Omega}_v^2$ must be real and non-negative. Furthermore, α_2 and α_3 must also be real so we require $\lambda^2 \geqslant 0$. Also, $\sin^2\theta$ must be in the range [0,1] so Eq. (68b) implies $0 \leqslant -\gamma_2/\gamma_1 \leqslant 1$. Finally, $\omega_p^2 \geqslant 0$ so from Eq. (66), $a_3/a_1 - \alpha_2 \bar{\Omega}_v^2 u \sin^2\theta \geqslant 0$.

1. The limit $a_2 \to a_1$

The equilibrium equation, Eq. (69), cannot be solved analytically except in some special cases. One important case is the limit $a_2 \to a_1$. In this case, $\gamma_2 = 0$ which, from Eq. (68b), implies $\theta = 0$ provided that $\gamma_1 \neq 0$. (We will assume that this is the case for now and return to the $\gamma_1 = 0$ case later.) For these equilibria, the tilt angle θ approaches zero as the plasma becomes spheroidal. This is the limit in which the rotating equilibria match onto the linear (2,1) normal modes of Refs. 5–7. In this case, Eq. (68a) implies $\delta_2 = 0$. The equation $\delta_2 = 0$ is, in fact, the dispersion relation for the linear (2,1) modes. Substituting for α_3 from Eq. (70) and taking $a_2 = a_1$ in Eq. (68d), the equation $\delta_2 = 0$ can be written as

$$1 - \frac{A_1}{A_3} + \frac{\bar{\Omega}_v^2}{2} u(1 - u \pm \lambda) = 0.$$

Since u depends on $\bar{\Omega}_v^2$ it is not useful to solve for $\bar{\Omega}_v^2(u, a_3/a_1)$. Instead, we take the term involving $\pm\lambda$ to the right-hand side and square both sides, substituting for λ^2 from Eq. (70c), which yields

$$\left(1 - \frac{A_1}{A_3} + \frac{\bar{\Omega}_v^2}{2} u(1-u)\right)^2 = \frac{\bar{\Omega}_v^2 u^2}{4}\left(u - \frac{a_3 + a_1}{a_3 - a_1}\right)\left(u - \frac{a_3 - a_1}{a_3 + a_1}\right).$$

The term involving u^4 cancels, so after multiplication by $\bar{\Omega}_v^2$ and substitution for u in terms of β using Eq. (67) this equation becomes a cubic polynomial in $\bar{\Omega}_v^2$:

$$(1-\beta)^3 + \left(1 - \frac{A_1}{A_3}\right)\left(-(1-\beta)^2 + \frac{\bar{\Omega}_v^2(1-\beta)}{(a_3/a_1)^2 - 1} + \frac{(1 - A_1/A_3)\bar{\Omega}_v^2}{[(a_3/a_1)^2 - 1]^2}\right) = 0 \tag{71}$$

[recall from Eq. (50) that β is linear in $\bar{\Omega}_v^2$]. The three solutions of Eq. (71) for $\bar{\Omega}_v^2(a_3/a_1, \bar{\Omega}_c^2)$ yield the linear frequencies of the three (2,1) modes through the equation $\bar{\omega} = (\pm|\bar{\Omega}_v| - \bar{\Omega}_c)/2$, since for these modes the linear frequency equals the rotation frequency ω of the nonlinear equilibria. There are two values of ω for each solution of Eq. (71), corresponding to the excitation of a linear mode around either of the rigid-rotor equilibria with given $\bar{\Omega}_c$ and a_3/a_1 described by Eq. (57). The equivalence of Eq. (71) to the linear dispersion relation, Eq. (10) of Ref. 6 or Eq. (5.15) of Ref. 7, can be easily verified. As was mentioned in the Introduction, when $\Omega_c \gg \omega_p$ two of the solutions of Eq. (71) describe plasma oscillations and the other is an upper hybrid mode.

In general, when $a_2 \neq a_1$, similar algebraic manipulations of the full equilibrium equation, Eq. (69), reveal that this equation can be written as a sixth-order polynomial in $\bar{\Omega}_v^2$; however, the form of the coefficients is extremely complicated so we do not reproduce them here. There are then six solutions for $\bar{\Omega}_v^2(a_2/a_1, a_3/a_1, \bar{\Omega}_c^2)$, which must be determined numerically. However, an extensive numerical parameter search of the solutions reveals that, for given parameter values, there are never more than three real solutions for $\bar{\Omega}_v^2$ which also satisfy the conditions $\omega_p^2 \geqslant 0$, $\lambda^2 \geqslant 0$, $\bar{\Omega}_v^2 \geqslant 0$, and $0 \leqslant \sin^2\theta \leqslant 1$. Furthermore, these physical solutions exist only for certain ranges of a_2/a_1, a_3/a_1, and $\bar{\Omega}_c^2$. This is analogous to the previously derived bounds on aligned equilibria given by Eq. (63); however, the bounds become more complicated for the tilted equilibria and, in particular, the ranges depend on which of the solutions of Eq. (69) that we consider. Fortunately, this rather complex situation is clarified by the existence of relatively simple analytic equations describing the "existence boundaries," or relations between $\bar{\Omega}_c^2$, a_2/a_1, and a_3/a_1, implied by the conditions $\lambda^2 = 0$, $\bar{\Omega}_v^2 = 0$, $\omega_p^2 = 0$, $\sin^2\theta = 0$ and $\sin^2\theta = 1$. [The other condition, $\mathrm{Im}(\bar{\Omega}_v^2) = 0$, cannot be determined analytically since no general analytic solution for a sixth-order polynomial is known.]

However, before we consider the general existence boundaries we examine one more simplifying limit, for which we can obtain analytic forms for the solutions of Eq. (69) as well as for the regions of existence.

2. The guiding-center limit

In experiments, the cyclotron frequency is often very large compared to all other frequencies in the dynamics so it is useful to consider the limit $\bar{\Omega}_c \gg 1$ in Eq. (69); that is, the guiding-center limit of the tilted ellipsoid equilibria. In this limit, the solution of Eq. (69) simplifies considerably. All three physical solutions can be found analytically in this limit, although only two correspond to guiding-center dynamics as the third involves motions at frequencies on the order of $\bar{\Omega}_c$.

The two guiding-center solutions are found by assuming that $\beta \sim O(\bar{\Omega}_c)$, and $\bar{\Omega}_v \sim O(\bar{\Omega}_c)$, so that Eq. (67) implies $u \sim O(1/\bar{\Omega}_c)$. In this case, only the $-$ branch of Eq. (70) provides a dominant balance in Eq. (69) that is consistent with this ordering assumption. For this branch we find that

$$\alpha_2 = -\frac{\beta a_3}{\bar{\Omega}_c^2 a_1} \quad \text{and} \quad \alpha_3 = -\frac{\beta a_2}{\bar{\Omega}_c^2 a_1}, \tag{72}$$

where we have used Eq. (67) and have kept only leading-order terms. Equations (72) imply that the internal fluid rotation is of $O(1)$ since $\bar{\Lambda}_i = \bar{\Omega}_v \alpha_i z_i$.

The angle of tilt of the ellipsoid can be obtained from either Eq. (68a) or (68b). Our ordering implies that $\gamma_1 \sim \bar{\Omega}_c^2 u$ and $\gamma_2 \sim \bar{\Omega}_c^2 u(a_2^2 - a_1^2)/(a_3^2 - a_2^2)$, so

$$\sin^2\theta = \frac{a_1^2 - a_2^2}{a_3^2 - a_2^2} + O\left(\frac{1}{\bar{\Omega}_c}\right). \tag{73}$$

From the conditions $0 \leqslant \sin^2\theta \leqslant 1$, we then infer that

$$\text{if} \quad \frac{a_2}{a_1} \geqslant (\leqslant) 1, \quad \text{then} \quad \frac{a_3}{a_1} \leqslant (\geqslant) 1 \tag{74}$$

in order that the solutions be physically relevant.

The rotation frequency of the ellipsoid can also be found by using Eqs. (72) to replace α_i in Eq. (69), again keeping only leading-order terms. We then obtain a linear equation in β^2, which can be solved in terms of $\bar{\Omega}_v^2$ via Eq. (50):

$$\frac{\beta^2}{\bar{\Omega}_c^2}\simeq\frac{(\bar{\Omega}_v^2-\bar{\Omega}_c^2)^2}{16\bar{\Omega}_c^2}=\frac{a_1^2(A_2-A_3)}{a_1^2(A_2-A_3)+a_3^2A_3-a_2^2A_2}+O\left(\frac{1}{\bar{\Omega}_c}\right). \tag{75}$$

Equations (72)–(75) provide two of the three possible physical solutions for tilted ellipsoids in the $\bar{\Omega}_c\gg 1$ limit. Note that, as for the aligned ellipsoids, each solution of Eq. (75) for $\bar{\Omega}_v^2$ corresponds to two possible rotation frequencies, $\bar{\omega}=(\pm|\bar{\Omega}_v|-\bar{\Omega}_c)/2$, and so there are four possible rotation frequencies, two of which correspond to guiding-center dynamics. We write these two guiding-center solutions out explicitly:

$$\bar{\omega}^2=\frac{a_1^2(A_2-A_3)}{a_1^2(A_2-A_3)+a_3^2A_3-a_2^2A_2}+O\left(\frac{1}{\bar{\Omega}_c}\right).$$

The rotation frequency of this tilted ellipsoid is independent of the cyclotron frequency (to lowest order in $1/\bar{\Omega}_c$) because in the laboratory frame the plasma moves only in the z direction. This can be seen by using Eq. (72) in Eqs. (18) and (14) in order to find the fluid velocity $\mathbf{v}'$. We then rotate to the laboratory frame using Eqs. (23) and (73), obtaining

$$\mathbf{v}(\mathbf{x}')=\omega\frac{(a_3^2-a_2^2)}{2a_1^2}\sin(2\theta)x_1\hat{\mathbf{z}}+O\left(\frac{1}{\bar{\Omega}_c}\right).$$

Although the fluid flows only in the $\hat{\mathbf{z}}$ direction, the motion is phased around the surface of the tilted ellipsoid in just such a way as to produce a rotation of the surface at frequency ω (recall that the tilt is in the 2–3 plane, and x_1 is a coordinate normal to this plane). These solutions are nonlinear versions of the (2,1) plasma oscillations described by Eq. (71) in the $\Omega_c\gg\omega_p$ limit.

Finally, the density of the ellipsoid can also be found by applying Eqs. (72), (73), and (75) to Eq. (66), from which we obtain

$$\bar{\omega}_p^2=2\frac{(a_3^2-a_2^2)}{a_1^2(A_2-A_3)+a_3^2A_3-a_2^2A_2}+O\left(\frac{1}{\bar{\Omega}_c}\right). \tag{76}$$

This relation implies non-negative values for $\bar{\omega}_p^2$ for all a_2/a_1 and a_3/a_1 values that satisfy Eq. (74). By the same token, the right-hand side of Eq. (75) is also non-negative for all $(a_2/a_1,a_3/a_1)$ in the region described by Eq. (74), so the solutions are physically meaningful in this region.

Turning to the third solution, we now assume $\beta\sim O(1)$, $\bar{\Omega}_v\sim O(\bar{\Omega}_c)$. Now Eqs. (50) and (67) imply $u\sim O(1/\bar{\Omega}_c^2)$, and only the + root of Eq. (70) provides a consistent dominant balance in Eq. (69). In this case, we find $\alpha_2=a_2/a_1$ and $\alpha_3=a_3/a_1$, and when these results are used in Eq. (69) and only leading-order terms are kept we find a linear equation for β with the following solution in terms of $\bar{\Omega}_v^2$:

$$\bar{\Omega}_v^2=\bar{\Omega}_c^2-6+\frac{4a_1^2(A_3-A_2)}{a_1^2(A_3-A_2)+a_2^2A_2-a_3^2A_3}+O\left(\frac{1}{\bar{\Omega}_c}\right).$$

There are then two possible solutions for $\bar{\omega}$, one of which corresponds to an $\mathbf{E}\times\mathbf{B}$ drift form, i.e., $\bar{\omega}\sim O(1/\bar{\Omega}_c)$. However, the fact that α_2 and α_3 are $O(1)$ implies that $\Lambda\sim O(\bar{\Omega}_c)$, so this motion cannot be described by $\mathbf{E}\times\mathbf{B}$ drift dynamics alone. This solution is a finite-amplitude upper hybrid mode.

The tilt angle of the ellipsoid with respect to $\hat{\mathbf{z}}$ follows from the limiting forms for γ_1 and γ_2. From Eqs. (68e) and (68f), $\gamma_1\sim\bar{\Omega}_c^2a_1^2(a_3^2-a_2^2)/a_2^2a_3^2$ and $\gamma_2\sim\bar{\Omega}_c^2(a_2^2-a_1^2)/a_2^2$. Equation (68b) then implies

$$\sin^2\theta=\frac{a_3^2(a_1^2-a_2^2)}{a_1^2(a_3^2-a_2^2)}+O\left(\frac{1}{\bar{\Omega}_c}\right).$$

When we apply the constraints $0\leqslant\sin^2\theta\leqslant 1$, we are again led to Eq. (75) for the ranges of a_2/a_1 and a_3/a_1 for which a physical solution exists.

Finally, when these results are substituted into Eq. (66) we find that the density of the ellipsoid is also given by Eq. (76), so all three tilted solutions have the same density and region of existence in the $\bar{\Omega}_c\gg 1$ limit.

3. Existence boundaries and tilted spheroids

The general solutions for the tilted ellipsoids are parametrized by the values of a_2/a_1, a_3/a_1, and $\bar{\Omega}_c$, and solutions exist only for certain ranges of these parameters. Thus, for given $\bar{\Omega}_c$, the boundaries of the regions of existence of solutions trace out curves in the $(a_2/a_1,a_3/a_1)$ plane. For example, we have just found that, for $\bar{\Omega}_c\gg 1$, physical solutions exist only within existence boundaries given by Eq. (74). We now consider the general behavior of these limiting curves. By symmetry of the equilibria with respect to relabeling of the two- and three-body axes, the curves must be symmetric under reflection in this plane about the $a_2=a_3$ line, provided that $\theta\to\pi/2-\theta$ as we reflect solutions about this line.

We first consider the existence curves determined by $\sin^2\theta=0$. Reflection of these curves about the $a_2=a_3$ line then gives us the curves defined by $\sin^2\theta=1$. We have already discovered one $\sin^2\theta=0$ curve; our discussion of the linear (2,1) modes revealed that, if $\gamma_1\neq 0$ as $a_2\to a_1$, then $\theta\to 0$, so $a_2=a_1$ is a $\theta=0$ curve. Another $\sin^2\theta=0$ curve can also be found by considering the relations between a_3/a_1, a_2/a_1, and $\bar{\Omega}_c^2$ implied by Eqs. (68a) and (68b) as $\theta\to 0$, which may be written as $\delta_2=0$ and $\gamma_2=0$. Assuming that $a_2\neq a_1$, the $\gamma_2=0$ relation implies

$$\bar{\Omega}_v^2\alpha_3=\frac{A_1-A_2}{A_3}\frac{a_1a_2}{a_2^2-a_1^2}, \tag{77}$$

which, when substituted into $\delta_2=0$, yields a simple equation for u in terms of a_2/a_1 and a_3/a_1:

$$u=\frac{A_2-A_3}{A_1-A_2}\frac{a_2^2-a_1^2}{a_1^2}. \tag{78}$$

However, Eqs. (50) and (67) imply a general relation between $\bar{\Omega}_v^2$, $\bar{\Omega}_c^2$, and u:

$$\bar{\Omega}_v^2=\frac{(6-\bar{\Omega}_c^2)(a_3^2-a_2^2)}{4a_1^2u-(a_3^2-a_2^2)}. \tag{79}$$

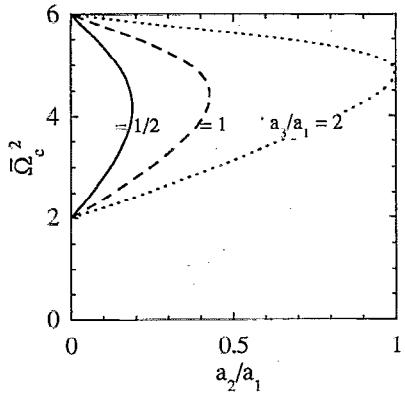

FIG. 9. Solutions of Eq. (81) for the $\sin^2\theta=1$ existence boundary. Solid line: $a_3/a_1=1/2$. Dashed line: $a_3/a_1=1$. Dotted line: $a_3/a_1=2$. Dashed line also gives the behavior of $\mathbf{C}_1$ as $\bar{\Omega}_c$ varies (see Fig. 13).

When Eqs. (78) and (79) are inserted into Eq. (77), we obtain

$$\bar{\Omega}_c^2=6-\frac{a_2/a_1}{\alpha_3 A_3}\left(\frac{4(A_2-A_3)}{(a_3/a_1)^2-(a_2/a_1)^2}-\frac{A_1-A_2}{(a_2/a_1)^2-1}\right). \tag{80}$$

Now, by Eq. (70b), $\alpha_3=\alpha_3(u,a_2/a_1,a_3/a_1)$, and Eq. (78) implies $u=u(a_2/a_1,a_3/a_1)$, so Eq. (80) gives $\bar{\Omega}_c^2(a_2/a_1,a_3/a_1)$ along the $\theta=0$ curve. It may be useful to note that, as $\theta\to 0$, $\alpha_2=\Lambda_2/(\sin\theta\bar{\Omega}_v)$ remains finite by Eqs. (78) and (70a), so Λ_2 also approaches zero in the limit. Thus, along the $\theta=0$ curve described by Eq. (80), the equilibrium approaches an aligned ellipsoid.

Finally, we note that symmetry under transposition of the two- and three-body axes labels implies that the $\theta=\pi/2$ curves are given by $a_1=a_3$, as well as the expression obtained by interchanging labels 2 and 3 in Eq. (80), which yields

$$\bar{\Omega}_c^2=6-\frac{a_3/a_1}{\alpha_2 A_2}\left(\frac{4(A_2-A_3)}{(a_3/a_1)^2-(a_2/a_1)^2}-\frac{A_1-A_3}{(a_3/a_1)^2-1}\right), \tag{81}$$

where we must also exchange the 2 and 3 labels in Eq. (78). The solution of Eq. (81) for $\bar{\Omega}_c^2$ as a function of a_2/a_1 are shown in Fig. 9 for several values of a_3/a_1. Along these curves one of the tilted ellipsoids attains $\theta=\pi/2$, becoming an aligned ellipsoid. Furthermore, as $a_3/a_1\to\infty$, Eq. (81) and (A8) imply that $\bar{\Omega}_c^2$ approaches either 6 or $2+a_2/a_1$, depending on whether one chooses the $-$ or $+$ branch for α_2 in Eq. (70a).

It is important to note that not all of the physical solutions pass through $\sin^2\theta=0$ along the $\theta=0$ curves (and naturally the same caveat applies to the $\theta=\pi/2$ curves). The full equilibrium equation has up to three physical solutions at any given $(\bar{\Omega}_c,a_2/a_1,a_3/a_1)$; however, Eqs. (66), (67), (77), and (78) imply that Eq. (80) picks out only one of these three solutions. The other two solutions do not pass through $\theta=0$ because they satisfy the general equilibrium equation and not just $\delta_2=\gamma_2=0$.

On the other hand, along the line $a_2=a_1$ we saw that $\theta=0$ for all three physical solutions, but only if $\gamma_1\neq 0$. These three solutions corresponded to the linear (2,1) normal modes. We will soon see that another condition, $\bar{\Omega}_v^2\geqslant 0$, limits the range of validity of these three solutions to a finite segment of the $a_2=a_1$ line; along this line the inequality $\Omega_v^2\geqslant 0$ is just the Brillouin limit condition [see Fig. 6 and Eq. (58)]. However, for a_3/a_1 values beyond this segment new solutions can occur that satisfy $\gamma_1=0$ (and that do not have $\theta=0$). We will now consider these solutions, which correspond to tilted spheroidal equilibria with internal fluid shears.

Taking $a_1=a_2$ in the expression $\gamma_1=0$ yields the following relation between u and a_3/a_1:

$$\frac{\bar{\Omega}_v^2\alpha_2}{a_3/a_1}\left[-u+\left(\frac{a_3}{a_1}\right)^2-1\right]=0.$$

Using Eq. (70a) one can easily show that $\alpha_2=0$ can occur only when $a_2\to 0$ or $u=0$, which are unimportant cases. We are left with the case $u=a_3^2/a_1^2-1$, which implies that $1-\beta-\bar{\Omega}_v^2=0$, or

$$\bar{\Omega}_v^2=2-\bar{\Omega}_c^2/3, \tag{82}$$

where we have used the definitions of u and β [see Eqs. (50) and (67)]. Recall that this condition occasioned an exception to Riemann's theorem (cf. Sec. III A). We will now see that the exception arises because of the existence of tilted spheroidal equilibria, which are degenerate cases in the proof since rotations of the body axes around the spheroid's axis of symmetry are allowed.

Equation (82) implies that these spheroidal equilibria exist only for $\bar{\Omega}_c^2\leqslant 6$, and we will soon see that solutions also exist only for $\bar{\Omega}_c^2\geqslant 3$. The condition $\bar{\Omega}_c^2\leqslant 6$, when applied to rigid-rotor solutions, would correspond to the regime of oblate rigid-rotor spheroids. However, the tilted spheroids must be prolate, as can be seen from the form of α_2 and α_3 when $u=a_3^2/a_1^2-1$ and $a_2=a_1$:

$$\alpha_2=(a_3/a_1\pm\sqrt{a_3^2/a_1^2-4})/2, \tag{83a}$$

and

$$\alpha_3=(2-a_3^2/a_1^2\pm a_3/a_1\sqrt{a_3^2/a_1^2-4})/2, \tag{83b}$$

which follow from Eqs. (70). The $\pm$ signs go together in these two equations, so there are two possible solutions. Equations (83) imply that $a_3/a_1>2$ is required for a physical equilibrium.

Furthermore, unlike the rigid-rotor spheroids, these spheroids are tilted with respect to the magnetic field; according to Eq. (68a)

$$\sin^2\theta=-\delta_2/\delta_1$$
$$=\frac{1-A_1/A_3+\alpha_3(a_3^2/a_1^2-1)(2-\bar{\Omega}_c^2/3)}{[\alpha_3-\alpha_2 a_1 A_1/(a_3A_3)](a_3^2/a_1^2-1)(2-\bar{\Omega}_c^2/3)}. \tag{84}$$

Tilt angles as a function of a_3/a_1 are displayed in Fig. 10(a) for various values of $\bar{\Omega}_c^2$ in the range $3\leqslant\bar{\Omega}_c^2\leqslant 6$ for which these spheroids exist. For $3\leqslant\bar{\Omega}_c^2<4.84$, two tilted spheroids may exist with the same shape a_3/a_1 but with

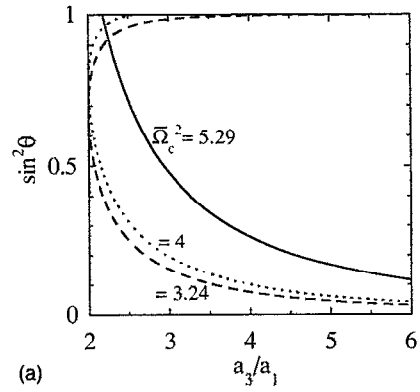

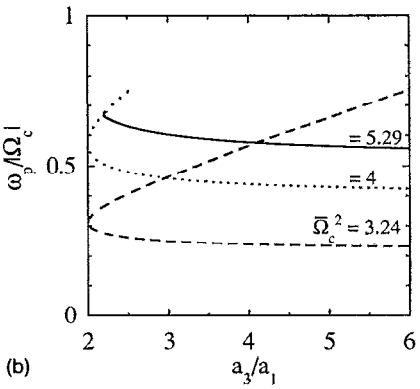

FIG. 10. Behavior of the tilted spheroids for three field strengths. Dashed line: $|\bar{\Omega}_c|=1.8$. Dotted line: $|\bar{\Omega}_c|=2$. Solid line: $|\bar{\Omega}_c|=2.3$. (a) shows the tilt angle θ of the spheroids and (b) displays the plasma frequency. In both figures, the lower branch corresponds to solution 5 of Fig. 13 and the upper branch corresponds to solution 4.

different tilt angles and densities. The densities are displayed in Fig. 10(b).

For $4.84<\bar{\Omega}_c^2<6$, only one equilibrium exists [corresponding to the + branch solution of Eqs. (83)] because the other solution has completely passed above the $\sin^2\theta=1$ limit. The value $\bar{\Omega}_c^2=4.84$ at which the − branch of Eq. (83) disappears can be obtained by determining the value of $\bar{\Omega}_c^2$ for which both $\sin^2\theta=1$ and $\lambda^2=0$. At this point, Eqs. (83) imply $\alpha_2=1$ and $\alpha_3=-1$, so by taking $a_3/a_1=2$, $\alpha_3=-1$, $\alpha_2=1$, and $a_2/a_1=1$ in Eq. (81) we find, after employing the spheroid relation $2A_1+A_3=2$, that $\bar{\Omega}_c^2$ must satisfy $\bar{\Omega}_c^2=4/A_1(2)$. If one uses the prolate spheroidal form of A_1, Eq. (A5), this result can be written in terms of elementary functions:

$$\bar{\Omega}_c^2=\frac{12}{4-(1/\sqrt{3})\ln[(2+\sqrt{3})/(2-\sqrt{3})]}=4.840\,06\cdots.$$

Furthermore, no tilted spheroids exist below $\bar{\Omega}_c^2<3$ because in this range $\omega_p^2<0$ for these solutions. This can be seen by substituting Eqs. (82)–(84) into the equation for ω_p^2, Eq. (66). However, this result applies not only to the tilted spheroids but to two entire branches of triaxial equilibria for which the tilted spheroids are the cylindrically

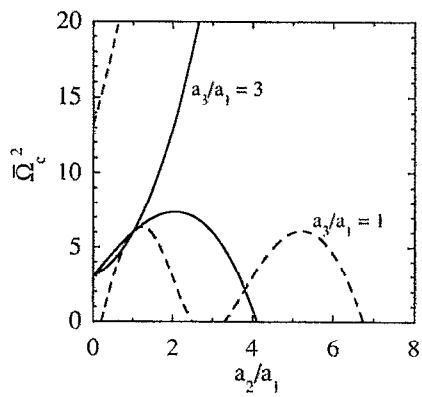

FIG. 11. Solutions of Eqs. (89) and (90) for the $\lambda^2=0$ existence boundaries for two values of a_3/a_1. Dashed line: $a_3/a_1=1$. Solid line: $a_3/a_1=3$.

symmetric limit, so we will now consider the more general derivation of the existence boundary corresponding to $\omega_p^2=0$.

This boundary may be obtained from Eq. (66):

$$\frac{\alpha_2}{a_3/a_1}\bar{\Omega}_v^2 u\sin^2\theta=1. \tag{85}$$

If we regard this as an equation for $\sin^2\theta$ and substitute the solution into Eq. (68a), several cancellations occur and we find that $\bar{\Omega}_v^2$ must satisfy the equation

$$\bar{\Omega}_v^2 u=\frac{a_3/a_1}{\alpha_2}-\frac{a_2/a_1}{\alpha_3}.$$

When this result, along with Eq. (85), is substituted into Eq. (68b), we find after several more cancellations that

$$u=(a_3^2-a_2^2)/a_1^2. \tag{86}$$

However, when this form for u is used in the preceding equation we find that the a_2/a_1 and a_3/a_1 dependencies cancel and we are left with the simple result $\bar{\Omega}_v^2=1$. Furthermore, a comparison of Eqs. (67) and (86) implies that $1-\beta=\bar{\Omega}_v^2$, and since $\bar{\Omega}_v^2=1$ we find that $\bar{\Omega}_c^2=3$ when $\omega_p^2=0$. Note that because α_2 is double valued Eq. (85) implies that up to two of the three possible physical solutions approach $\omega_p^2=0$ as $\bar{\Omega}_c^2\to 3$. In fact, these two equilibria correspond, for $a_2=a_1$, to the two tilted spheroids.

Turning now to the curves defined by $\lambda^2=0$, we see from Eq. (70c) that $\lambda^2=0$ implies

$$u=\frac{a_3\pm a_2}{a_3\mp a_2}, \tag{87}$$

and in either the + or − case $\alpha_2=(1+u)/(2a_3/a_1)$, and $\alpha_3=(1-u)/(2a_2/a_1)$. Substituting Eq. (87) into these relations yields

$$\alpha_2=\frac{a_1}{a_3\mp a_2}\quad\text{and}\quad\alpha_3=\frac{a_1}{a_2\mp a_3}. \tag{88}$$

Then substitution of Eqs. (87) and (88) into Eq. (69) results in a linear equation for $\bar{\Omega}_v^2$ whose solution is

$$\bar{\Omega}_v^2(r_2,r_3)=-(r_3\mp r_2)^2\frac{(2r_3+r_3r_2^2\pm r_2\mp r_2r_3^2)A_3+(\pm 2r_2\pm r_2r_3^2+r_3-r_3r_2^2)A_2-2(r_3\pm r_2)}{(r_3^3-3r_3\mp r_2\mp r_2r_3^2)A_3+(\pm r_2^3\mp 3r_2-r_3-r_3r_2^2)A_2+2(r_3\pm r_2)}, \tag{89}$$

where we have introduced the notation $r_2=a_2/a_1$ and $r_3=a_3/a_1$ in order to save space. This result, along with Eq. (87), can be employed in Eq. (79) to obtain $\bar{\Omega}_c^2$ along the $\lambda^2=0$ curves:

$$\bar{\Omega}_c^2\left(\frac{a_2}{a_1},\frac{a_3}{a_1}\right)=6-\left(\frac{4a_1^2}{(a_3\mp a_2)^2}-1\right)\bar{\Omega}_v^2\left(\frac{a_2}{a_1},\frac{a_3}{a_1}\right), \tag{90}$$

where the $\pm$ signs go together in Eqs. (89) and (90). Note that this solution has the proper symmetry upon interchange of labels 2 and 3. The solutions for $\bar{\Omega}_c^2$ are plotted in Fig. 11 as a function of a_2/a_1 for various values of a_3/a_1. One can see that, for any given value of $\bar{\Omega}_c^2$, there may be several $\lambda^2=0$ curves running through the $(a_2/a_1,a_3/a_1)$ plane. Fortunately, it turns out that only two of these curves will be required to determine the regimes of existence of physical solutions, and these two curves are reflections of one another about the $a_2=a_3$ line so only one really need be considered. The other curves are superceded by one or more of the other existence conditions, or merely reflect a continuation of a solution from the + branch to the − branch of Eqs. (70). We will further find that these $\lambda^2=0$ curves contribute to the existence boundaries only when $3<\bar{\Omega}_c^2<6$. We will discuss this in more detail presently, when we plot the existence curves in the $(a_2/a_1,a_3/a_1)$ plane.

The final boundaries to be considered analytically are determined by the condition $\bar{\Omega}_v^2=0$. In this limit, Eq. (67) implies that $u\to\infty$, and there are two possibilities for α_2 and α_3. Either

$$\alpha_3\simeq-\frac{u}{a_2/a_1}+\frac{a_3^2a_1}{a_2(a_3^2-a_2^2)}+O(\bar{\Omega}_v^2),$$

and

$$\alpha_2\simeq\frac{a_3a_1}{a_3^2-a_2^2}+O(\bar{\Omega}_v^2),$$

or

$$\alpha_2\simeq\frac{u}{a_3/a_1}+\frac{a_2^2a_1}{a_3(a_3^2-a_2^2)}+O(\bar{\Omega}_v^2),$$

and

$$\alpha_3\simeq\frac{-a_2a_1}{a_3^2-a_2^2}+O(\bar{\Omega}_v^2).$$

For the former case in which $\alpha_3\to\infty$ as $\bar{\Omega}_v^2\to 0$, Eq. (68a) implies that

$$\frac{(a_3^2-a_2^2)}{a_2^2}\frac{(1-\beta)^2}{\bar{\Omega}_v^2}(\sin^2\theta-1)+\sin^2\theta(1-\beta)\left(\frac{A_2}{A_3}-\frac{a_3^2}{a_2^2}\right)$$
$$+1-\frac{A_2}{A_3}+(1-\beta)\frac{a_3^2}{a_2^2}=O(\bar{\Omega}_v^2), \tag{91}$$

where we have used the definition of u. Then to lowest order in $\bar{\Omega}_v^2$, only the first term contributes and we find that $\sin^2\theta=1$. We then substitute $\sin^2\theta=1$ in Eq. (68b) and keep only the lowest-order terms as $\bar{\Omega}_v^2\to 0$ to obtain

$$\frac{A_2-A_1}{A_3}-\frac{A_2+A_3-A_1}{A_3}(1-\beta)=O(\Omega_v^2).$$

Thus, β satisfies $\beta=A_3/(A_2+A_3-A_1)$, or in terms of $\bar{\Omega}_c^2$,

$$\bar{\Omega}_c^2=2+\frac{4A_3}{(A_2+A_3-A_1)}, \tag{92}$$

where Eq. (50) has been employed. Equation (92) gives a curve along which a tilted ellipsoid attains $\bar{\Omega}_v^2=0$.

However, since this is an existence boundary we must keep the next-order term in Eq. (91) to determine whether $\sin^2\theta$ will be larger than or less than unity as $\bar{\Omega}_v^2\to 0^+$. We will now show that this constraint implies that Eq. (92) is only valid when $a_3/a_1\leqslant 1$. By linearizing Eq. (91) in the small quantity $1-\sin^2\theta$, we find that this quantity satisfies

$$1-\sin^2\theta=\frac{a_2^2a_1^2}{(a_3^2-a_2^2)^2}\frac{\bar{\Omega}_v^2}{(1-\beta)^2}\left(\beta\frac{A_2}{A_3}-1\right).$$

Thus, in order that $\sin^2\theta\leqslant 1$ as $\bar{\Omega}_v^2\to 0^+$, we require

$$\beta\leqslant A_3/A_2.$$

If we now substitute Eq. (92) into this relation, we find that a_2/a_1 and a_3/a_1 must satisfy the condition

$$\frac{A_3-A_1}{A_2+A_3-A_1}\geqslant 0.$$

Since $A_3\geqslant A_1$ only when $a_3\leqslant a_1$, this condition is satisfied only where either $a_3\leqslant a_1$, or $A_3-A_1+A_2\leqslant 0$. However, in the latter case $\omega_p^2\leqslant 0$, as we now show. The plasma frequency is found by taking $\sin^2\theta=1$, $\bar{\Omega}_v^2=0$ in Eq. (66) and substituting for $\bar{\Omega}_c^2$ via Eq. (92). The result is

$$\bar{\omega}_p^2=\frac{2\beta}{A_3}=\frac{2}{A_2+A_3-A_1}.$$

Thus, if $A_3-A_1+A_2\leqslant 0$, $\bar{\omega}_p^2\leqslant 0$, and so Eq. (92) describes a physical $\bar{\Omega}_v^2=0$ equilibrium only for $a_3\leqslant a_1$.

If we now return to the other case where α_3 remains finite and $a_2\to\infty$ as $\bar{\Omega}_v^2\to 0$, we find after a similar analysis that the equation for the existence boundary is identical to Eq. (91) except that the 2 and 3 labels are interchanged and now $\sin^2\theta\to 0$ rather than unity along the boundary. This $\bar{\Omega}_v^2=0$ curve is

$$\bar{\Omega}_c^2=2+\frac{4A_2}{(A_2+A_3-A_1)}, \tag{93}$$

and $a_2\leqslant a_1$ is required for a physical solution. This existence boundary is shown in Fig. 12 as a function of a_2/a_1 for three values of a_3/a_1.

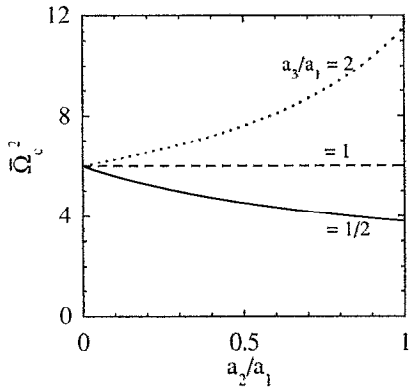

FIG. 12. Solutions of Eq. (93) for $\bar{\Omega}_v^2 = 0$ existence boundaries for three values of a_3/a_1. Solid line: $a_3/a_1 = 1/2$. Dashed line: $a_3/a_1 = 1$. Dotted line: $a_3/a_1 = 2$.

For a certain range of $\bar{\Omega}_c^2$ the two $\bar{\Omega}_v^2 = 0$ existence boundaries cross in the $(a_2/a_1, a_3/a_1)$ plane; that is, there are values of a_2/a_1 and a_3/a_1 which satisfy Eqs. (92) and (93) simultaneously. Since the two equations are symmetric under interchange of the 2 and 3 labels, this crossing must occur at some point where $A_2 = A_3$, which implies $a_2 = a_3$. An equation for the crossing point then follows from either Eq. (92) or Eq. (93), along with Eq. (A4):

$$A_1 = \frac{\bar{\Omega}_c^2 - 4}{\bar{\Omega}_c^2 - 3}, \tag{94}$$

where A_1 is evaluated for $a_2 = a_3$. Furthermore, the crossing of the $\bar{\Omega}_v^2$ curves can occur only where both curves are valid, i.e. $a_3 \leqslant a_1$ and $a_2 \leqslant a_1$. However, in this regime Eq. (A4) implies $0 \leqslant A_1 \leqslant 2/3$, and Eq. (94) then implies that a crossing of the curves occurs only for $\bar{\Omega}_c^2$ in the range $4 \leqslant \bar{\Omega}_c^2 \leqslant 6$.

4. The regions of existence

We are now ready to consider the form of the regions of existence of tilted equilibria in the $(a_2/a_1, a_3/a_1)$ plane as a function of $\bar{\Omega}_c^2$. We employ the analytic forms for the existence boundaries derived in the previous subsection as well as numerical solutions of Eq. (69) in order to determine the topology of the regions of existence as a function of $\bar{\Omega}_c^2$. The existence boundaries determine where a physical solution vanishes, and the numerical solutions of Eq. (69) allow us to track this solution from one boundary to another, thus identifying the region of the $(a_2/a_1, a_3/a_1)$ plane in which the solution exists. The regions have different topologies depending on whether $\bar{\Omega}_c^2 \geqslant 6$, $6 \geqslant \bar{\Omega}_c^2 \geqslant 4$, $4 \geqslant \bar{\Omega}_c^2 \geqslant 3$, or $3 \geqslant \bar{\Omega}_c^2 \geqslant 2$, and examples of each are shown in Fig. 13. These topologies can be understood from the analytic behavior of the existence boundaries, as we will see. For $\bar{\Omega}_c^2 \leqslant 2$, there are no tilted ellipsoids, just as for the case of the aligned ellipsoids.

The regions of existence for $\bar{\Omega}_c^2 \geqslant 6$ are shown in Figs. 13(a) and 13(b) for the cases $\bar{\Omega}_c^2 = 16$ and $\bar{\Omega}_c^2 = 6.25$. The behavior of the solutions in this regime is also plotted in Fig. 14, which shows the solutions along a line through the $(a_2/a_1, a_3/a_1)$ plane. Figure 14(a) illustrates that solutions with plasma densities elevated well above the Brillouin limit can occur for plasmas that are sufficiently disklike, just as for the aligned ellipsoids. Here, however, these high-density disk equilibria are tilted with respect to the magnetic field [see Fig. 14(c)].

Figures 13 are symmetric about the line $a_2 = a_3$, as expected from symmetry under interchange of the (2,3) body axes. The points **M** and **M′** are the Brillouin limit beyond which rigid-rotor spheroidal equilibria cease to exist. Point **M** is determined by Eq. (58), and the behavior of **M** as $\bar{\Omega}_c^2$ varies can be taken from Fig. 6. Along the line segments [(1,0),**M**] or [(0,1),**M′**], the equilibria become the usual rigid-rotor spheroids, described by Eq. (44), with an infinitessimal tilt (2,1) linear perturbation added that rotates at one of the three frequencies given by the solution of Eq. (71). On the former line segment, $\sin^2\theta \to 0$, and $\sin^2\theta \to 1$ on the latter, and furthermore ω_p^2 approaches the same rigid-rotor equilibrium value for all three solutions.

The line segments [(1,0), **M**] and [(0,1),**M′**] are also existence boundaries for the three solutions that describe the conditions $\sin^2\theta = 0$ and $\sin^2\theta = 1$, respectively. A numerical examination of the solutions on either side of [(1,0),**M**] and [(0,1),**M′**] reveals that, in the regime $\bar{\Omega}_c^2 \geqslant 6$, all three equilibria exist only to the left of (**S**,**M**) and below (**S**,**M′**), where the point **S** corresponds to a spherical equilibrium. This region of existence agrees with the $\bar{\Omega}_c \gg 1$ limiting form of the existence region, given by Eq. (74). However, this limiting form breaks down near the points **M** or **M′**, where the rotation frequency approaches $\Omega_c/2$. Indeed, at the point **M**, the condition $\sin^2\theta = 0$ is superceded by $\bar{\Omega}_v^2 = 0$ along curve A [described by Eq. (93)], as well as the condition $\mathrm{Im}(\bar{\Omega}_v^2) = 0$. This latter condition is satisfied along curve B, which is found by numerically solving Eq. (69) for $\bar{\Omega}_v^2$ and determining at what values of $(a_2/a_1, a_3/a_1)$ the solution is no longer real. Along curve B, $\mathrm{Im}(\bar{\Omega}_v^2)$ becomes nonzero for two solutions, which we call solutions 1 and 2; solution 1 has the larger value of $|\bar{\Omega}_v|$. These two solutions must therefore merge and disappear along B and one can see this behavior in Fig. 14. Thus the regime of existence of solutions 1 and 2 is delineated by the $a_2/a_1 = 0$ axis, and the curves [(0,1),**S**], [**S**,**M**], and B—that is, the gray area of Fig. 13(a). The other solution, solution 3, has a larger region of existence delineated by the $a_2/a_1 = 0$ axis and the curves [(0,1),**S**], [**S**,**M**] and A—the horizontally lined region. When $\Omega_c \gg \omega_p$ solutions 1 and 3 become the plasma oscillations of Eq. (75), and solution 2 is the upper hybrid oscillation.

We note that various $\lambda^2 = 0$ curves also run through the $(a_2/a_1, a_3/a_1)$ plane, as described by Eqs. (89) and (90). However, a solution that disappears on one side of the $\lambda^2 = 0$ curve is replaced on the other side by a solution on the opposite branch of α_2 and α_3 with the same physical properties and we regard these two branches as the same solution. These unimportant $\lambda^2 = 0$ curves are not shown; we display only those curves that contribute to the existence boundaries.

The next figure in the sequence, Fig. 13(b), is still in the first regime $\bar{\Omega}_c^2 \geqslant 6$, but is plotted for a lower cyclotron

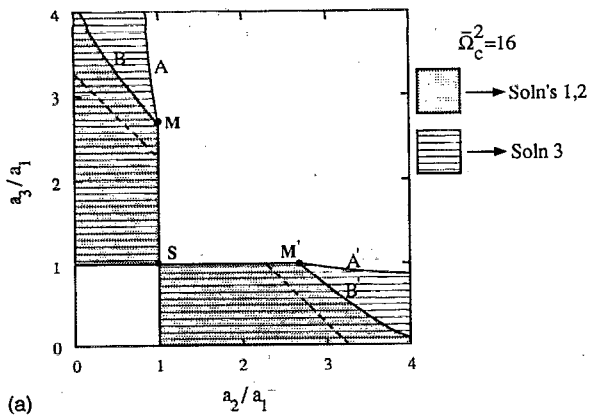

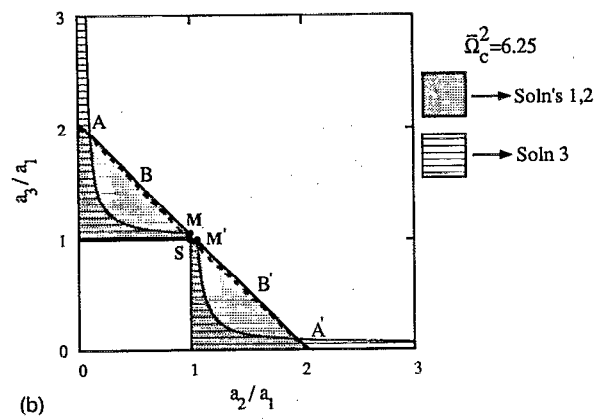

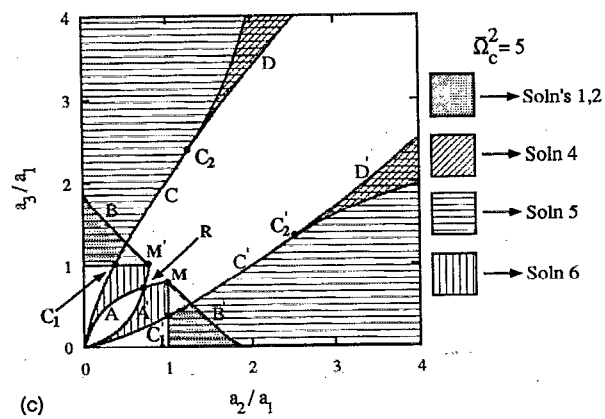

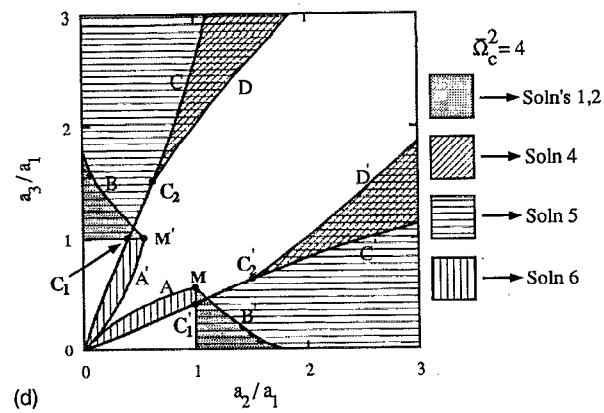

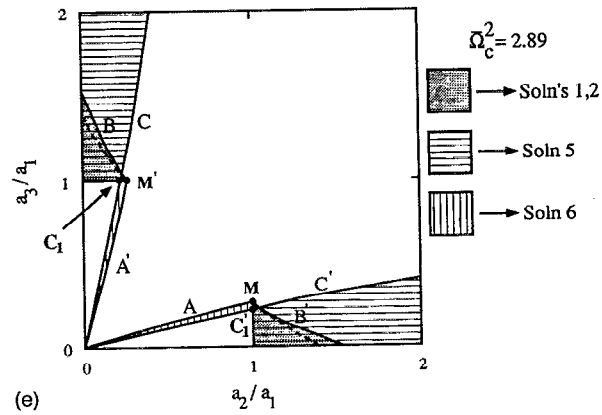

FIG. 13. Existence regions for the tilted ellipsoids, plotted in the $(a_2/a_1, a_3/a_1)$ plane for five values of the normalized cyclotron frequency $\bar{\Omega}_c$. Regions of existence are bounded by the lines $a_2/a_1=1$ and $a_3/a_1=1$, as well as by the solid curves labeled A–D and their mirror images in the $a_2=a_3$ line, A′–D′. Along curve A, $\bar{\Omega}_v=0$ and $\theta=0$ for solutions 3 and 6. Along curve B, solutions 1 and 2 merge and disappear as Im $\bar{\Omega}_v^2$ becomes nonzero. Along curve C, $\theta=\pi/2$ for solutions 4 and 6, and for solution 5 below $\mathbf{C}_2$. Along curve D, $\lambda^2=0$ for solutions 4 and 5. Special points are **M**, the Brillouin limit; **S**=(1,1), the spherical limit; the points **R**, $\mathbf{C}_1$, and $\mathbf{C}_2$ (which are points of intersection of the existence boundaries); and their primed counterparts below the $a_2=a_3$ line. The dashed lines [which are difficult to see in (c) and (d) because of their proximity to curves B and B′] provide the triaxial shape required for a Dedekind ellipsoid solution at the given values of $\bar{\Omega}_c^2$. (a) $\bar{\Omega}_c^2$=16. (b) $\bar{\Omega}_c^2$=6.25. (c) $\bar{\Omega}_c^2$=5. (d) $\bar{\Omega}_c^2$=4. (e) $\bar{\Omega}_c^2$=2.89.

frequency given by $\bar{\Omega}_c^2=6.25$. As one can see, as $\bar{\Omega}_c^2$ nears 6, the points **M** and **M′** approach **S** [see Eq. (58) for the spherical case $A_3=2/3$, and see Fig. 6]. Furthermore, the $\bar{\Omega}_v^2=0$ curves labeled A and A′ push the existence of solution 3 into an ever-decreasing area (see Fig. 12, which shows this behavior as a function of $\bar{\Omega}_c^2$). As $\bar{\Omega}_c^2\to 6^+$, solution 3 approaches $\bar{\Omega}_v^2=0$ except along the line [(1,0),M], where $\bar{\Omega}_v^2$ takes on the finite values associated with a linear mode. Thus the behavior of solution 3 is quite singular in the limit $\bar{\Omega}_v^2\to 6$. Solutions 1 and 2, which are bounded by curve B, also exist in a smaller (but finite) region of the plane as $\bar{\Omega}_c^2\to 6$.

As $\bar{\Omega}_c^2$ drops below 6, the character of the existence regions changes. The topology of the regions is displayed in Fig. 13(c) for the case $\bar{\Omega}_c^2=5$, and for this cyclotron frequency the solutions are displayed in Fig. 15 along the line $a_3/a_1=0.6$. Here, we concentrate only on the region for which $a_3\geqslant a_2$ in order to simplify the discussion, since the region $a_3<a_2$ may be obtained by reflection. As $\bar{\Omega}_c^2\to 6^-$, curves A and A′ suffer a discontinuous change. For $\bar{\Omega}_c^2\to 6^+$, curve A approaches the line segments $[(0,1),(0,\infty)]$ and [(0,1),(S)]. However, as $\bar{\Omega}_c^2\to 6^-$, the former segment is replaced by [(0,0),(0,1)]. This behavior can be extracted by eye from Fig. 12. As $\bar{\Omega}_c^2$ decreases further, the two curves A and A′ emerge from these limiting cases as shown in Fig. 13(c). The two curves cross along the $a_2=a_3$ line at the point **R**, described by Eq. (94). Furthermore, a $\sin^2\theta=1$ curve now appears, which we call

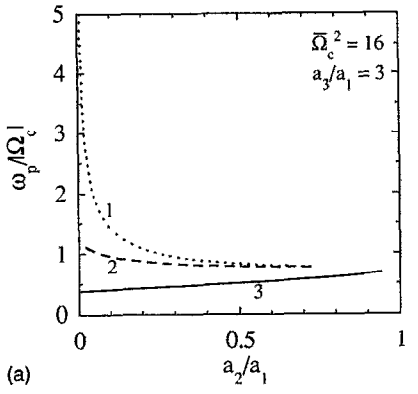

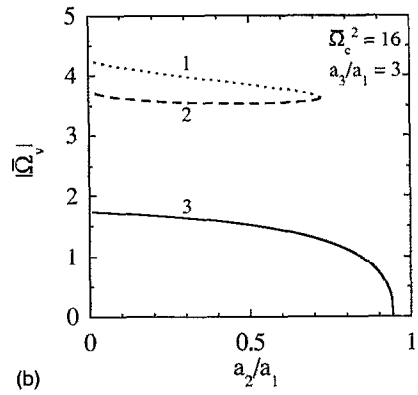

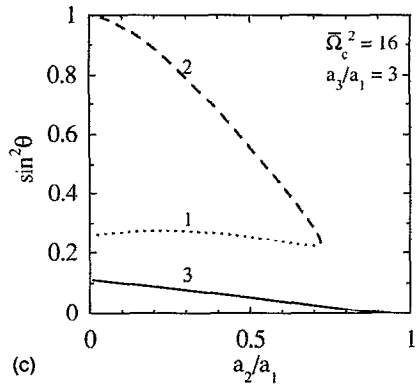

FIG. 14. Behavior of the tilted ellipsoids as a_2/a_1 varies for $\bar{\Omega}_c^2=16$ and $a_3/a_1=3$ [i.e., along the line $a_3/a_1=3$ in Fig. 13(a)]. Solutions are labeled 1, 2, and 3 [see text and Fig. 13(a)]. (a) shows the plasma frequency of the solutions, normalized to the cyclotron frequency in order to compare to the Brillouin limit. (b) shows the vortex frequency of the solutions, and (c) the tilt angle of the three-body axis with respect to the magnetic field.

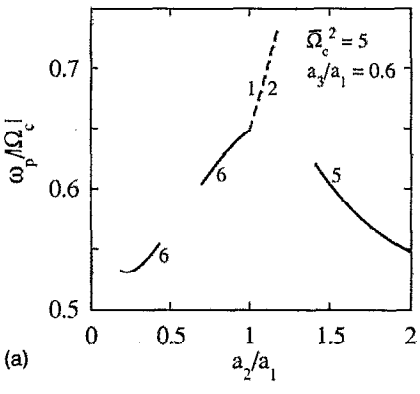

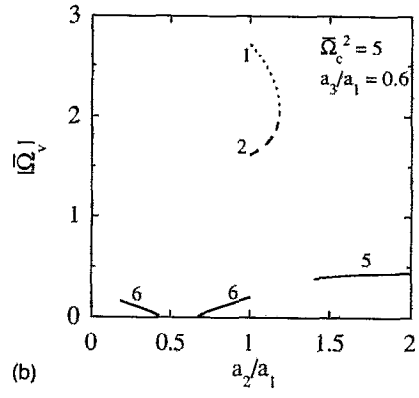

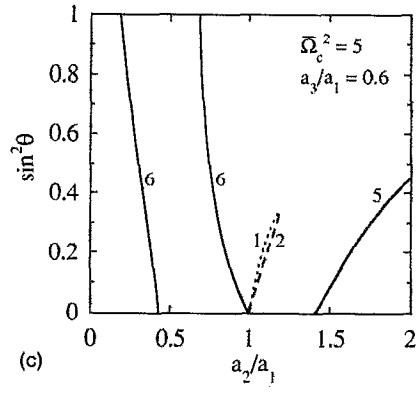

FIG. 15. Behavior of the tilted ellipsoids as a_2/a_1 varies for $\bar{\Omega}_c^2=5$ and $a_3/a_1=0.6$ [i.e., along the line $a_3/a_1=0.6$ in Fig. 13(c)]. Solutions are labeled 1, 2, 5, and 6 [see text and Fig. 13(c)]. In (a), solutions 1 and 2 have nearly the same plasma frequency.

curve C (see Fig. 9, which shows that $\bar{\Omega}_c^2$ must be less than 6 in order for this existence boundary to appear). This curve intersects the rigid-rotor equilibria at $\mathbf{C}_1$. The dependence of $\mathbf{C}_1$ on $\bar{\Omega}_c^2$ is given by the dashed line in Fig. 9. For $a_3/a_1 \gg 1$, curve C approaches the line $a_2/a_1=\bar{\Omega}_c^2-2$. This follows from the limiting form of the $\sin^2\theta=1$ curve discussed in the paragraph following Eq. (81). Finally, a segment of one of the $\lambda^2=0$ curves (curve D) becomes an existence boundary, intersecting C at $\mathbf{C}_2$. The behavior of $\mathbf{C}_2$ as $\bar{\Omega}_c^2$ varies is shown in Fig. 16.

Three new solutions appear within these new boundaries, replacing solution 3. One of the three solutions, solution 4, is bounded by the triangular region between curves C and D—the diagonally lined area. It approaches $\sin^2\theta=1$ along C and merges with another new solution, solution 5, as λ approaches zero along curve D. Solution 5 can be regarded as a smooth continuation of solution 3, reappearing from the $a_2=0$ axis as $\bar{\Omega}_c^2$ drops below 6. Solution 5 approaches $\sin^2\theta=1$ only along curve C below $\mathbf{C}_2$, since only one solution approaches this limit and solution 4 has already done so above $\mathbf{C}_2$. Above $\mathbf{C}_2$, solution 5 extends out to curve D where it merges with solution 4. Thus it exists in the area delineated by the $a_2=0$ axis, and the

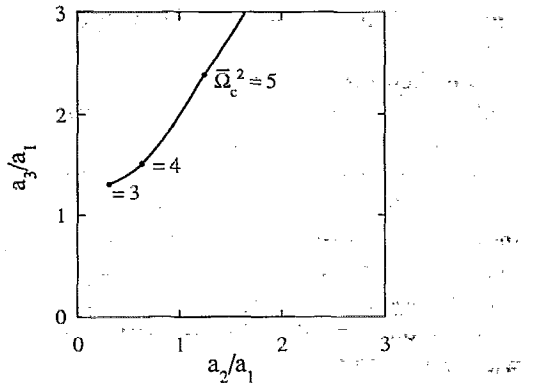

FIG. 16. Behavior of the point $\mathbf{C}_2$ as $\bar{\Omega}_c^2$ varies. As $\bar{\Omega}_c^2 \to 6$, $\mathbf{C}_2 \to (\infty,\infty)$. The points 3, 4, and 5 mark the position of $\mathbf{C}_2$ for these values of $\bar{\Omega}_c^2$.

curves $[(1,0),\mathbf{C}_1]$, $[\mathbf{C}_1,\mathbf{C}_2]$, and D—the horizontally lined area. We also note that, along the line $a_2=a_1$, solutions 4 and 5 become the tilted spheroid equilibria shown in Fig. 11. The third new solution, solution 6, is also a continuation of solution 3 but it exists for $a_3<a_1$ in the region bounded by the curves $[(0,0),\mathbf{C}_1]$, $[\mathbf{C}_1,\mathbf{M}]$, $[\mathbf{M},\mathbf{R}]$, and $[\mathbf{R},(0,0)]$—the vertically lined region. Finally, solutions 1 and 2 are now bounded in the region determined by the a_2/a_1 axis, curve B and the line segment $[(0,1),\mathbf{M}']$. The behavior of these solutions along the line $a_3/a_1=0.6$ is shown in Fig. 15.

As $\bar{\Omega}_c^2$ falls below 4, the point **R** disappears into the origin [see Eq. (94)] and the region of existence of solution 6 changes, being delineated now by the curves $[(0,0),\mathbf{C}_1]$, $[\mathbf{C}_1,\mathbf{M}']$, and A′. This behavior is displayed in Fig. 13(d).

This topology of the regions of existence is preserved until $\bar{\Omega}_v^2$ falls below 3, where there is another discontinuous change in behavior. As $\bar{\Omega}_v^2 \to 3$, solutions 4 and 5 approach $\omega_p^2=0$, in accord with the discussion surrounding Eq. (85). Solution 4 disappears when $\bar{\Omega}_c^2<3$, and solution 5 becomes bounded on the right by curve C, the $\sin^2\theta=1$ line. Its region of existence is now delineated by the $a_2/a_1=1$ axis as well as the curves $[(0,1),\mathbf{C}_1]$, and C. Since curve C no longer crosses the $a_2=a_1$ line when $\bar{\Omega}_c^2<3$ the tilted spheroids disappear, as we discussed previously. Solutions 1, 2, and 6 remain in their respective existence regions. Finally, as $\bar{\Omega}_c^2 \to 2$, $\mathbf{M}'$ and $\mathbf{C}_1$ move toward the point (0,1) and all of the regions of existence merge into the $a_2/a_1=0$ line. Below $\bar{\Omega}_c^2=2$, there are no more equilibria, as was the case for the aligned ellipsoids.

5. Dedekind ellipsoids

The physical solution of Eq. (69), which we have labeled solution 1 in the figures, has an important property. For a given value of $\bar{\Omega}_c$ there exist particular values of a_2/a_1 and a_3/a_1 for which the rotation frequency of this equilibrium is identically zero; that is, the tilted ellipsoid appears to be stationary in the laboratory frame, although internal motions remain. This stationary equilibrium can be observed in both Figs. 14(b) and 15(b) at the point where the cyclotron and vortex frequencies are equal. This equilibrium is of particular importance in experiments since it can resonantly interact with a static external field asymmetry.[5–7] Fluid ellipsoids whose bounding surface is stationary but which have internal motions are referred to as the Dedekind ellipsoids in the astrophysics literature.[12,14]

Once it is recognized that such stationary solutions exist, characterizing them is relatively straightforward. The solution by assumption has $\omega=0$, which implies $\bar{\Omega}_v^2=\bar{\Omega}_c^2$ and $\beta=-1/2$. In turn, this implies through Eq. (67) that

$$u=\frac{3}{2}\frac{(a_3^2-a_2^2)}{\bar{\Omega}_c^2}.$$

We substitute this result as well as Eqs. (70) into the general equilibrium equation, Eq. (69), and isolate on one side of the equation those terms that are linear in the square-root term, λ. Then on squaring both sides, we are left after some algebra with a cubic equation for $\bar{\Omega}_c^2$ of the form

$$\sum_{i=0}^{3} c_i \bar{\Omega}_c^{2i}=0. \tag{95}$$

The coefficients c_i are rather complicated:

$$\begin{aligned}
c_0=&\tfrac{27}{16}(1-A_1/A_3+3A_2/A_3)(3-A_1/A_3+A_2/A_3)\\
&\times(a_2^2-a_3^2)^2,\\
c_1=&-\tfrac{9}{4}\{2A_2/A_3[(a_2^2+a_3^2)a_1^2+4(a_2^2-a_3^2)^2]\\
&+A_1/A_3(1-A_2/A_3)(a_3^2-a_2^2)(2+a_2^2-3a_3^2)\\
&+(A_2/A_3)^2[(3a_3^2-5a_2^2)a_1^2+2(a_2^2-a_3^2)^2+a_2^4\\
&-a_3^4]+(3a_2^2-5a_3^2)a_1^2+2(a_3^2-a_2^2)^2-a_3^4-a_2^4\},\\
c_2=&\tfrac{3}{4}\{2A_2/A_3\{3[a_2^4+a_3^4-a_1^4+2(a_3^2+a_2^2)a_1^2]-7a_2^2a_3^2\}\\
&+2A_1/A_3(1-A_2/A_3)(a_3^2-a_2^2)+(A_2/A_3)^2\\
&\times[3(a_1^4-a_2^4)+4(a_3^2-4a_2^2)a_1^2-2a_2^2a_3^2]\\
&+3(a_1^4-a_3^4)+4(a_2^2-4a_3^2)a_1^2-2a_3^2a_2^2\},\\
c_3=&-(1-A_2/A_3)a_1^2[a_1^2-A_2/A_3(a_1^2-3a_2^2)-3a_3^2].
\end{aligned}$$

These coefficients have been checked using the algebra manipulator MATHEMATICA. This cubic equation for $\bar{\Omega}_c^2$ has three roots, all three of which can be real and positive, depending on the choice of a_2/a_1 and a_3/a_1. However, only one of these three roots corresponds to a physical solution—solution 1. We have checked the other two roots of Eq. (95) numerically over a large range of values of a_2/a_1 and a_3/a_1 and have found no cases for which these roots correspond to physical solutions. The values of a_2/a_1 and a_3/a_1 for which the rotation frequency of solution 1 vanishes are shown in Fig. 13 as dotted lines. For $\bar{\Omega}_c^2<6$, one can see that the lines closely follow curve B, and the point of intersection of these lines with the spheroidal equilibria is near M, the Brillouin limit. This behavior is due to the rapid variation in $\bar{\Omega}_v^2$ as solutions 1 and 2 merge, as can

be seen in Fig. 15(b). The dotted lines are partially obscured by curve B in Figs. 13(c) and 13(d). We also note in passing that the spherical case $a_1=a_2=a_3$ can be solved analytically since c_3 and c_0 are zero in this limit, and $A_1=A_2=A_3=2/3$. The solution of Eq. (95) is then $|\bar{\Omega}_c|=5/2$, the case plotted in Fig. 13(b).

IV. CONCLUSIONS

We have shown that nonlinear quadrupole oscillations of a homogeneous non-neutral plasma ellipsoid can be analyzed as a relatively simple Hamiltonian system with nine degrees of freedom, following from a reduction of the pressureless Euler equations for an ideal cold fluid. The constants of the motion were found, and the special case of cylindrically symmetric oscillations in the length and radius of a spheroidal plasma were analyzed in detail, and in the limit of large cyclotron frequency this motion was reduced to quadratures. The predicted nonlinear frequency shifts should be experimentally observable.

The equilibria of the general equations were analyzed and were shown to fall into two classes. The aligned ellipsoids have a principal axis oriented along the magnetic field and the fluid velocity is perpendicular to **B**. The tilted ellipsoids contain fluid flows that are no longer perpendicular to **B**; instead $\omega \| \mathbf{B}$, but $\Lambda \nparallel \mathbf{B}$ and these vectors fall in a principal plane of the ellipsoid. Simple forms for the equilibria were found in the experimentally relevant limit $|\bar{\Omega}_c| \gg 1$. The regions of parameter space $(a_2/a_1, a_3/a_1, \bar{\Omega}_c)$ for which equilibrium solutions exist were analyzed and a surprisingly varied range of equilibria was found, including tilted spheroids and disks, as well as triaxial ellipsoids that are stationary in the lab frame. For given values of the parameters, two aligned equilibria were found, corresponding to finite-amplitude versions of the two (2,2) quadrupole normal modes. Up to three tilted equilibrium solutions were found, and the topology of the regions of existence in the $(a_2/a_1, a_3/a_1)$ plane was shown to fall into four classes, depending on whether $\bar{\Omega}_c^2 \geqslant 6$, $6 \geqslant \bar{\Omega}_c^2 \geqslant 4$, $4 \geqslant \bar{\Omega}_c^2 \geqslant 3$, or $3 \geqslant \bar{\Omega}_c^2 \geqslant 2$. These topologies are displayed in Fig. 13.

In both the aligned and tilted equilibria, solutions were found that exceed the Brillouin density limit. Such solutions are possible because the plasma does not rotate rigidly. High-density equilibria should also occur for certain sheared plasma flows in more complicated geometries than those considered here. For example, a finite-amplitude $l=2$ diocotron mode set up in any plasma that is already near the Brillouin limit should produce some density compression. This effect may be observable in present experiments.[19]

In this paper, we have not considered the stability of the nonlinear quadrupole motions with respect to small perturbations. For example, ideal fluid instabilities such as Kelvin–Helmholtz shear flow instabilities will no doubt occur if the fluid shear in the ellipsoid is sufficiently large. However, such instabilities generally have a finite threshold for onset, so it is possible that finite-sized quadrupole distortions of the cloud may be observable experimentally. This important question will be considered in future papers.

Furthermore, throughout the paper we have considered only a cylindrically symmetric time-independent external trap field in order to simplify the analysis. However, time dependences and asymmetries can be kept without changing the general equations, Eqs. (22), provided that these fields remain of the quadrupole form given by Eq. (4a). For example, the effect of a squeeze field, in which all three diagonal components of ϵ_e are different, can be taken into account; and the effect of a tilt of the magnetic field with respect to the trap electrodes adds off-diagonal terms to ϵ_e. The effect of these field errors on the equilibrium and dynamics of ellipsoidal non-neutral plasmas will be considered in future papers.

ACKNOWLEDGMENTS

The author gratefully acknowledges useful discussions with Dr. C. F. Driscoll and Dr. K. S. Fine.

This work was supported by National Science Foundation Grant No. PHY87-06358 and ONR Grant No. N00014-89-J-1714.

APPENDIX A: ELECTROSTATIC POTENTIAL WITHIN A HOMOGENEOUS ELLIPSOID

The plasma potential ϕ_p satisfies the Poisson equation

$$\nabla^2 \phi_p = -4\pi q n, \tag{A1}$$

whereas the gravitational potential ϕ_G satisfies the similar equation, $\nabla^2 \phi_G = 4\pi G m n$. This implies that a self-gravitating system of masses has the same potential as a system of charges interacting via Coulomb's law, if we identify $G \leftrightarrow -q/m$. We can therefore directly apply known results for the potential within a homogeneous self-gravitating ellipsoidal mass to determine the potential ϕ_p within a homogeneous single-species ellipsoidal plasma. Chapter 3 of Ref. 14 provides a list of useful relations.

The potential ϕ_p is quadratic, taking the following simple form in the body-axis coordinates $\mathbf{x}'$:

$$\phi_p(\mathbf{x}') = -\frac{1}{4}\frac{m}{q}\omega_p^2(A_1 x_1^2 + A_2 x_2^2 + A_3 x_3^2) + \frac{1}{4}\frac{m}{q}\omega_p^2 I, \tag{A2}$$

where $\omega_p^2 = 4\pi q^2 n/m$ is the square of the plasma frequency, $A_i = A_i(a_2/a_1, a_3/a_1)$ and $I(a_2/a_1, a_3/a_1)$ is a constant that is chosen to match the interior potential onto an exterior solution that approaches zero at large distances. The value of this constant is

$$I = \sum_{i=1}^{3} A_i a_i^2. \tag{A3}$$

Since ϕ_p satisfies Poisson's equation, substitution of Eq. (A2) into (A1) yields the relation

$$A_1 + A_2 + A_3 = 2. \tag{A4}$$

The functional form of the A_i's is particularly simple when the ellipsoid is a spheroid. For a prolate spheroid with $a_1=a_2<a_3$,

$$A_1(a_3/a_1)=\frac{1-e^2}{e^2}\left[\frac{1}{1-e^2}-\frac{1}{2e}\ln\left(\frac{1+e}{1-e}\right)\right],$$
$$A_2=A_1\,, \tag{A5}$$
$$A_3(a_3/a_1)=2\frac{1-e^2}{e^2}\left[\frac{1}{2e}\ln\left(\frac{1+e}{1-e}\right)-1\right],$$

where $e=\sqrt{1-a_1^2/a_3^2}$. For an oblate spheroid, the analytic continuation of A_i's into the regime $a_1=a_2>a_3$ yields

$$A_1(a_3/a_1)=\frac{\sqrt{1-e'^2}}{e'^2}\left(\frac{\arcsin e'}{e'}-\sqrt{1-e'^2}\right),$$
$$A_2=A_1\,, \tag{A6}$$
$$A_3(a_3/a_1)=2\frac{\sqrt{1-e'^2}}{e'^2}\left(\frac{1}{\sqrt{1-e'^2}}-\frac{\arcsin e'}{e'}\right),$$

where here $e'=\sqrt{1-a_3^2/a_1^2}$. For a general triaxial ellipsoid with $a_1>a_2>a_3$, the A_i's can be written in terms of elliptic integrals:

$$A_1(a_2/a_1,a_3/a_1)=2\frac{a_2a_3}{a_1^2}\frac{F(\theta,k)-E(\theta,k)}{k^2\sin^3\theta},$$
$$A_2(a_2/a_1,a_3/a_1)$$
$$=2\frac{a_2a_3}{a_1^2}\frac{E(\theta,k)-k'^2F(\theta,k)-(a_3/a_2)k^2\sin\theta}{k^2k'^2\sin^3\theta}, \tag{A7}$$
$$A_3(a_2/a_1,a_3/a_1)=2\frac{a_2a_3}{a_1^2}\frac{(a_2/a_3)\sin\theta-E(\theta,k)}{k'^2\sin^3\theta},$$

where

$$k=\sqrt{\frac{a_1^2-a_2^2}{a_1^2-a_3^2}},$$
$$k'^2=1-k^2,$$

and

$$\theta=\arccos(a_3/a_1).$$

In the limit that one principal axis becomes very long, these functional forms simplify considerably. By taking $a_3/a_1\to\infty$, a_2/a_1 finite, the following limiting forms are found, good for all values of a_2/a_1:

$$A_3=0,$$
$$A_1=\frac{2a_2}{a_1+a_2}, \tag{A8}$$
$$A_2=\frac{2a_1}{a_1+a_2}.$$

Finally, a simple result relating derivatives of the A_i's follows from a consideration of the energy required to produce an infinitesimal deformation of the ellipsoid:

$$a_i\frac{\partial I}{\partial a_i}=I-A_ia_i^2. \tag{A9}$$

APPENDIX B: LIST OF SYMBOLS AND NOTATION

N: number of ions;
T: temperature;
n: density;
λ_D: Debye length;
q: ion charge;
ω_p: plasma frequency;
Ω_c: cyclotron frequency;
$\mathbf{B}$: magnetic field vector;
m: ion mass;
ϕ_e: external trap potential;
ω_z: single particle axial bounce frequency;
$\hat{\mathbf{z}}$: unit vector in the direction of the trap axis and magnetic field;
$\boldsymbol{\omega}$: ellipsoid rotation frequency vector;
$\mathbf{x}=(x,y,z)$: position vector measured from the center of the cloud in the laboratory frame of reference;
$\mathbf{x}'=(x_1,x_2,x_3)$: position vector measured with respect to principal (body) axes;
(a_1,a_2,a_3): lengths of the principal axes of the ellipsoid;
$(\hat{\mathbf{e}}_1,\hat{\mathbf{e}}_2,\hat{\mathbf{e}}_3)$: unit vectors in the directions of the principal axes;
(ϕ,θ,ψ): Euler angles;
$\mathbf{v}$: fluid velocity vector;
ζ: internal vorticity vector;
(ϕ_f,θ_f,ψ_f): internal fluid Euler angles;
t: time;
$\mathbf{E}$: electric field vector;
ϕ_p: space-charge potential;
ϵ_e: external electric field tensor;
ϵ_p: self-electric field tensor;
$A_i(a_2/a_1,a_3/a_1)$, $A_i(a_3/a_1)$: general form and spheroidal form, respectively, of the normalized space-charge electric field components along the principal axes;
$\mathbf{W}$: velocity tensor;
$\mathbf{l}$: unit tensor;
$\mathbf{S}$: ellipsoid shape tensor;
$\mathbf{R}$: ellipsoid rotation tensor;
Λ: internal fluid rotation frequency vector;
Ω_v: vortex frequency vector;
(z_1,z_2,z_3): components of $\hat{\mathbf{z}}$ in body axes;
$\mathscr{L}$: Lagrangian;
$\mathscr{A}$: vector potential;
$\mathscr{K}$: kinetic energy;
$\mathscr{M}$: magnetic energy;
$\mathscr{P}$: potential energy;
V: plasma volume;
p_u: momentum conjugate to any coordinate u;
$\mathbf{L}$: canonical angular momentum vector;
$\mathbf{F}$: internal fluid rotation tensor;
$(\hat{\mathbf{e}}_{f1},\hat{\mathbf{e}}_{f2},\hat{\mathbf{e}}_{f3})$: internal fluid unit vectors;
$\mathbf{C}$: canonical circulation vector;
$d\mathbf{S}$: area element;
$\mathscr{H}$: Hamiltonian;
K_1,K_2: linear combinations of constants p_ϕ and p_{ϕ_f};

$\mathscr{H}_s$: spheroidal Hamiltonian;
$\mathscr{H}_\parallel$: parallel energy;
$\phi_{\rm eff}$: effective parallel potential energy;
$\mathscr{H}_\parallel^{\rm min}$: minimum parallel energy;
ω_{20}: frequency of spheroidal plasma oscillation;
p,p_0: plasma pressure;
γ: ratio of specific heats;
C': constant in the equation of state;
β: trap parameter;
α_i: ratio of components of internal fluid rotation frequency and vortex frequency;
D,E: coefficients in aligned ellipsoid equilibrium equation;
$\beta_1^{(2)}$: functions of a_1,a_2, and a_3 employed in derivation of Eq. (61);
$u,\delta_1,\delta_2,\gamma_1,\gamma_2,\lambda$: parameters in the equations for tilted ellipsoids;
c_i: coefficients in the equation for a Dedekind ellipsoid.

Throughout the paper, a prime ($'$) on a vector or tensor denotes a particular representation in which components are taken with respect to the principal axes. The components of any vector $\mathbf{v}'$ are v_i, $i=1$–3, corresponding to components in the directions of the three-body axis unit vectors $\hat{\mathbf{e}}_i$. The subscript r on a vector or matrix implies that it is evaluated in a noninertial frame rotating with the body axes. An asterisk (*) on any matrix, such as $\boldsymbol{\omega}^*$, implies that it is antisymmetric and has the following relation with its dual $\boldsymbol{\omega}$:

$$\boldsymbol{\omega}^* = -\boldsymbol{\omega}' \times \mathbf{I}.$$

An overbar ($\bar{\cdot}$) denotes normalization. Times are normalized by ω_z^{-1}, distances are normalized by $a_0=(3Nq^2/n\omega_z^2)^{1/3}$, and masses are normalized by $Nm/5$.

[1] L. R. Brewer, J. D. Prestage, J. J. Bollinger, W. M. Itano, D. J. Larson, and D. J. Wineland, Phys. Rev. A **38**, 859 (1988).
[2] J. H. Malmberg and T. M. O'Neil, Phys. Rev. Lett. **39**, 1071 (1977).
[3] J. J. Bollinger and D. J. Wineland, Phys. Rev. Lett. **53**, 348 (1984).
[4] L. Turner, Phys. Fluids **30**, 3196 (1987).
[5] D. J. Heinzen, J. J. Bollinger, F. L. Moore, W. M. Itano, and D. J. Wineland, Phys. Rev. Lett. **66**, 2080 (1991).
[6] D. H. E. Dubin, Phys. Rev. Lett. **66**, 2076 (1991).
[7] J. J. Bollinger, D. J. Heinzen, F. L. Moore, W. M. Itano, D. J. Wineland, and D. H. E. Dubin, "Electrostatic modes of a Penning trap plasma," submitted to Phys. Rev. A.
[8] C. M. Surko, M. Leventhal, and A. Passner, Phys. Rev. Lett. **62**, 901 (1989); M. D. Tinkle, T. J. Murphy, and C. M. Surko, Bull. Am. Phys. Soc. **36**, 2334 (1991).
[9] G. Gabrielse, X. Fei, L. A. Orozoco, R. J. Tjoelker, J. Haas, H. Kalinowsky, T. A. Trainor, and W. Kells, Phys. Rev. Lett. **63**, 1360 (1989).
[10] R. C. Davidson, *Physics of Non-Neutral Plasmas* (Addison–Wesley, Redwood City, CA, 1990), p. 42.
[11] L. D. Landau and E. M. Lifshitz, *Fluid Mechanics* (Pergamon, New York, 1989), p. 12.
[12] S. Chandrasekhar, *Ellipsoidal Figures of Equilibrium* (Yale University Press, New Haven, 1969).
[13] S. A. Prasad and T. M. O'Neil, Phys. Fluids **22**, 278 (1979).
[14] J. Binney and S. Tremaine, *Galactic Dynamics* (Princeton University Press, Princeton, NJ, 1987).
[15] R. C. Davidson, *Theory of Non-Neutral Plasmas* (Benjamin, Reading, MA, 1974), p. 8.
[16] H. Goldstein, *Classical Mechanics* (Addison–Wesley, Redwood City, CA, 1950), p. 109.
[17] H. Goldstein, in Ref. 16, p. 369.
[18] T. M. O'Neil, Phys. Fluids **23**, 2216 (1980).
[19] C. F. Driscoll and K. S. Fine, Phys. Fluids B **2**, 1359 (1990).
[20] H. Lamb, *Hydrodynamics*, 6th ed. (Dover, New York, 1932), p. 232.
[21] R. C. Davidson, in Ref. 15, p. 62.
[22] A. E. H. Love, Proc. London Math. Soc. **25**, 18 (1893).